Journal of Scientific Computing, Vol. 18, No. 3, June 2003 (© 2003)

A Numerical Study on Large-Time Asymptotics of the Lifshitz–Slyozov System

J. A. Carrillo[1] **and Thierry Goudon**[2]

Received April 15, 2002; accepted (in revised form) October 16, 2002

We numerically investigate the long time behavior of solutions of the Lifshitz–Slyozov system. We propose a numerical scheme in which the numerical dissipation is controlled in such a way that the results for large time are meaningful. In this respect, we find the long time behavior to crucially depend on the distribution of largest aggregates present in the solution. This fact proved, in some particular cases in [23], was difficult to obtain with previous numerical schemes in the engineering literature leading to wrong statements. We propose a numerical scheme in which we can observe and quantify the equilibration rates towards the right asymptotic profile. Moreover, this system appears to be a very interesting test problem for any anti dissipative scheme for conservation laws.

KEY WORDS: Lifshitz–Slyozov system; coagulation-fragmentation models; phase transition; WENO schemes; conservation laws.

1. INTRODUCTION

We focus on the asymptotic behavior of the solutions (c, f) of the following Lifshitz–Slyozov (LS) equations

$$\begin{cases} \dfrac{\partial f}{\partial t}+\dfrac{\partial}{\partial x}\left[(a(x)\,c(t)-b(x))\,f\right]=0 \qquad \text{in } \mathbb{R}_t^+\times\mathbb{R}_x^+, \\ c(t)+\displaystyle\int_{\mathbb{R}^+} xf(t,x)\,dx=\rho>0, \\ f_{|t=0}=f_0 \qquad \text{in } \mathbb{R}_x^+, \qquad c_{|t=0}=c_0. \end{cases} \tag{1.1}$$

[1] Departamento de Matemática Aplicada, Universidad de Granada, 18071 Granada, Spain. E-mail: carrillo@ugr.es

[2] Laboratoire J. A. Dieudonné, UMR 6621, Université Nice-Sophia Antipolis, Parc Valrose, F-06108 Nice cedex 02, France and INRIA-Sophia, project CAIMAN. E-mail: goudon@math.unice.fr

0885-7474/03/0600-0429/0 © 2003 Plenum Publishing Corporation

This equation has been introduced in [18] as a model for the formation of a new phase in solid solutions. It is intended to describe the later stages of formation of the new phase: there still exists a non negligible number of precipitates having a supercritical size. In the earlier stages, fluctuations effects lead to the formation of these crystal germs. Here, the evolution of the precipitates is described through the density $f(t, x)$ of clusters having, at time t, the size $x \geqslant 0$. The dynamics is governed by a mechanism of removal from or addition to the clusters of free particles whose size is infinitely small compared to the size of the aggregates. These free particles are called "monomers," and their density at time t is denoted by $c(t)$. Note however that the model requires in these ordering properties that the size of the aggregates remains small compared to the average distance between clusters; consequently, encounters and coalescence effects are neglected in this approximation.

The quantity $V(t, x) = a(x)\, c(t) - b(x)$ is interpreted as the growth rate, at time t, for a cluster having size x. The given coefficients $a, b \geqslant 0$ are thus the rates at which monomers are added to or removed from the cluster, respectively. The first relation in (1.1) is a conservation law in size space, whereas the second relation is a constraint expressing the conservation of the total mass of the material within the solution. The crucial assumption on the coefficients is the existence, at any time t, of a unique critical size $x_{c(t)}$ which splits the size domain:

$$V(t, x) = a(x)\, c(t) - b(x) < 0, \qquad \text{for} \quad 0 \leqslant x < x_{c(t)},$$

$$V(t, x) = a(x)\, c(t) - b(x) > 0, \qquad \text{for} \quad x > x_{c(t)}.$$

Indeed, in deriving the rate of growth one considers the energy balance for a macro-particle, viewed as isolated in a bath of monomers, to maintain its size. Then, there is a competition between surface effects which tend to reduce the energetic cost due to the formation of an interface with volume effects associated to the bulk free energy of the cluster. The former are the dominating effects for small clusters. Accordingly, the evolution of a x-cluster is determined by the ratio between the monomers concentration $c(t)$ and an equilibrium concentration $c_e(x)$ characterized by the size x. It appears that $c_e(x)$ is a decreasing function of the size: there is a energetic advantage for the small grains to dissolve and transfer their mass to the large clusters. This phenomenom is known as the Ostwald ripening [20]: large grains are growing at the expense of smaller ones. From a technical point of view, this physical feature also explains why no boundary condition is needed at $x = 0$: the rate of growth $V(t, x)$ for small grains is negative. If one considers, at least formally, the characteristic curves

$$\frac{d}{dt} X(t; s, x) = V(t, X(t; s, x)), \qquad X(s; s, x) = x \tag{1.2}$$

then, they are pointing outside the domain $(0, +\infty)$ when they reach the origin. Precise form of the coefficients depends on the mechanism of mass transfer; assuming it is driven by diffusion, [18] gives the following coefficients

$$a(x) = x^{1/3}, \qquad b(x) = 1.$$

The critical size is therefore $x_{c(t)} = c^{-3}(t)$ in this case. Our study will be restricted to this physically relevant case. For details on the model, we refer of course to the original paper of Lifshitz–Slyozov [18], but one may also consult the classical reference [17] and the recent review of Sagalovich–Slyozov [25].

Mathematical results establishing existence-uniqueness of solutions for (1.1) have been obtained recently, by using various approaches: we refer to Niethammer and Pego [21], Collet and Goudon [7], Laurençot [14],... . On the other hand, derivation of (1.1) from the discrete model of Becker–Döring, an infinite system of ode's describing earlier stages of the new phase formation (see [2]), is discussed by Penrose [24], Collet *et al.* [9]. However, the asymptotic behavior of the solution of (1.1) is not well understood yet, in contrast with the situation concerning discrete models for which we refer to Ball *et al.* [1]. In their seminal paper [18], Lifshitz–Slyozov argue on physical grounds the following conjectures:

CLS1 The monomers concentration $c(t)$ decreases as time goes to infinity; precisely, c goes to 0 and behaves as $Kt^{-1/3}$, where K is a universal constant, independent on the initial state of the system.

CLS2 The total number of the agglomerates, that is

$$m_0(t) = \int_{\mathbb{R}^+} f(t, x)\, dx$$

behaves as Ct^{-1}, C depending on K and ρ, the total mass of the system.

CLS3 The mean radius

$$R_m(t) = \frac{1}{m_0(t)} \int_{\mathbb{R}^+} x^{1/3} f(t, x)\, dx$$

diverges in time like $t^{1/3}/K$.

CLS4 The solution $f(t, x)$ tends to a universal asymptotic profile, independently on the shape of the initial data: from the initial

state, it only depends on ρ as a scale parameter. Therefore, the solution forgets its initial shape.

Despite recent progresses, the question of the asymptotic behavior is not completely closed. In [10], an entropy has been exhibited for (1.1). Then, assuming that part of the support of the initial data f_0 is situated on the right of the initial critical point, we can prove that $c(t)$ goes to 0. But monotonicity is not obtained. On the other hand, while the $t^{-1/3}$ law for $c(t)$ (first part of conjecture CLS1) is not contested (it has been verified experimentally) the questions of uniqueness of the value of K, and uniqueness and stability of the final attractor have originated a controversial debate.

A first numerical study was performed in [6], leading to the conclusion that the conjecture CLS4 was true. The distributions taken as initial data in [6] were unbounded in support and the numerical scheme was a simple up-winding method for hyperbolic scalar equations. This conclusion has been proved to be wrong.

In particular, it was argued that the tail of the initial data and the largest particles play a crucial role and can modify the asymptotic profile. We refer for instance to Brown [3], Meerson and Sasorov [19] for a discussion on physical grounds. Mathematical analysis has been performed by Carr and Penrose [4], Niethammer and Pego [22] that indicated that the asymptotic behavior highly depends on the tip of the support of the initial data. Actually, these papers are concerned with a slightly modified model, the Lifshitz–Slyozov–Wagner equation, see [29]. However, this variant of (1.1) is interesting enough since, roughly speaking, it should be close to (1.1) when c has become small, see [15]. This analysis has been extended very recently to the system (1.1) by Niethammer and Pego [23]. In particular, according to [19, 22], and [23], starting from a compactly supported initial data with

$$f_0(x) \sim (x_s - x)^a, \qquad a > -1,$$

x_s being the endpoint of the support, the system cannot converge to the profile predicted by Lifshitz–Slyozov. Instead, one expects the convergence towards another profile, for a different value of K, defined by the value of the exponent a. This fact leads to the conclusion that the conjecture CLS4 written in that generality is false. From another point of view, Niethammer and Pego [23] results complement conjecture CLS4. Furthermore, according to a counterexample in [4], one certainly can find initial data (with high oscillations in the distribution of largest particles) for which the system does not converge to any asymptotic profile. Note however that [18] is certainly dealing with initial data having unbounded support and quite smooth tails.

In this paper, we propose a numerical scheme which is able to capture the right asymptotic behavior of the solution in contrast with some numerical results available in the literature. The general conclusion of our numerical study is that the behavior predicted by Lifshitz–Slyozov cannot be expected for any initial data. Some assumptions on the initial repartition of the aggregates in size seems necessary for c going to 0; and, then, the asymptotic state highly depends on the largest particles in the solutions. Actually, these results are in complete agreement with the results proved in [19, 22, 23]. However, with our numerical scheme we can check several other facts not covered by the results in [23]; convergence towards the smooth LS profile for unbounded support distribution functions, precise form of the convergence of $c(t)$, equilibration rates for the scaled equation,... . Moreover, this system is shown to be a very good test case for anti-dissipative numerical methods for conservation laws since very small errors in the approximation leads to wrong profiles in the long time asymptotics. Let us remark that the main contribution of this study is a detailed numerical classification of the asymptotic behavior of the LS system based on a suitable high order scheme.

The paper is organized as follows. In Sec. 2, we briefly recall some basic facts about equation (1.1). In Sec. 3, we introduce a scaled version of (1.1), which is appropriate to investigate the large time behavior of the system as shown in [23]. From the rescaled equation, we discuss the possible asymptotic states. Then, in Sec. 4, we describe in detail the results of our numerical investigation of (1.1). The final section is devoted to comments and conclusions on the study.

2. BASIC PROPERTIES OF LS

Let us start with some basic remarks. In the following, we use the characteristics associated to the growth rate, neglecting the technical difficulties caused by the blow up of the derivative at $x = 0$. As in [7], it allows us to write the solution as

$$f(t, x) = f_0(X(0; t, x))\, J(0; t, x) \tag{2.1}$$

where $J(s; t, x) = D_x X(s; t, x)$. Based on the characteristic form, we conclude:

1. The zeroth order moment, interpreted as the total number of clusters in the solution, reads, by using characteristics,

$$\int_{\mathbb{R}^+} f(t, x)\, dx = \int_{X(0; t, 0)}^{\infty} f_0(x)\, dx.$$

As a consequence of $V(t, 0) < 0$, we realize that $D_t X(0; t, 0) > 0$. Therefore

$$m_0 : t \longmapsto \int_{\mathbb{R}^+} f(t, x)\, dx \quad \text{is a non increasing function of time.}$$

The main effect of the equation is to "stretch" the initial data: it is expected that "mass goes to infinity," clusters in the solution having larger and larger size. From [18], it is expected that m_0 behaves as t^{-1}.

2. The time derivative of the monomer concentration, is given by

$$\frac{dc}{dt} = -\int_{\mathbb{R}^+} V(t, x)\, f(t, x)\, dx$$

$$= -\int_0^{x_{c(t)}} V(t, x)\, f(t, x)\, dx - \int_{x_{c(t)}}^{\infty} V(t, x)\, f(t, x)\, dx.$$

The first term is non negative, the second is non positive. Hence, there is a struggle between these terms, depending on the repartition of the clusters in size to determine the variation of $c(t)$.

3. It can be shown that $c(t) > 0$ for any time t. Next, if the initial data f_0 has its support in $[0, x_s]$; then, by using the formula (2.1), we realize that the support of the solution is contained in $[0, X(t; 0, x_s)]$. In particular, for $x_s < \infty$, the support of the solution remains bounded by $X(t, 0, x_s) < \infty$. If initially the endpoint x_s of the support of the initial data satisfy $x_s > x_{c_0}$; then the critical size cannot reach the end of the support: $X(t; 0, x_s) - x_{c(t)} > 0$ (see [10]).

4. According to [10], we expect that the total number of clusters $m_0(t)$ goes to 0 while the monomers concentration either tends to 0 or ρ. In particular, if there exists $\delta > 0$ such that $\mathrm{supp}(f_0) \cap [x_{c_0} + \delta, \infty[\neq \varnothing$, then $c(t) \to 0$. It is conjectured, for an initial data having its support in $[0, x_{c_0}]$, that the two behaviors: $c(t)$ goes to 0 or to ρ, are possible, depending crucially on the initial repartition of mass in the interval. We will see numerically that the two behaviors are indeed possible (see Figs. 7 and 8 later).

It is also worth saying some words on a variant of Eq. (1.1) which is commonly used. The Lifshitz–Slyozov–Wagner equation deals with a

situation where c has reached indeed an equilibrium: it is small enough to be neglected in the mass conservation relation, which becomes

$$\int_{\mathbb{R}^+} xf(t, x)\, dx = \rho$$

i.e., a constraint on the first moment. However, we keep the c in the definition of the growth rate and the evolution equation still reads

$$\frac{\partial f}{\partial t} + \frac{\partial}{\partial x}\left[(a(x)\, c(t) - b(x))\, f\right] = 0$$

Integrating the equation after multiplication by x, and taking into account the constraint, one sees that c should satisfy

$$c(t) = \int_{\mathbb{R}^+} b(x)\, f(t, x)\, dx \left(\int_{\mathbb{R}^+} a(x)\, f(t, x)\, dx\right)^{-1}.$$

For the coefficients of [18], we recover

$$c(t) = \int_{\mathbb{R}^+} f(t, x)\, dx \left(\int_{\mathbb{R}^+} x^{1/3} f(t, x)\, dx\right)^{-1} = \frac{1}{R_m(t)},$$

i.e., the inverse of the mean radius of the agglomerates. Summarizing, the Lifshitz–Slyozov–Wagner (LSW) problem is to solve

$$\begin{cases} \dfrac{\partial f}{\partial t} + \dfrac{\partial}{\partial x}\left[(a(x)\, c(t) - b(x))\, f\right] = 0 \qquad \text{in } \mathbb{R}_t^+ \times \mathbb{R}_x^+, \\ c(t) = \displaystyle\int_{\mathbb{R}^+} b(x)\, f(t, x)\, dx \left(\int_{\mathbb{R}^+} a(x)\, f(t, x)\, dx\right)^{-1} \\ f_{|t=0} = f_0 \qquad \text{in } \mathbb{R}_x^+, \qquad c_{|t=0} = c_0. \end{cases} \tag{2.2}$$

It can be proved that the LSW equation (2.2) can be obtained from the LS one (1.1) by an asymptotic argument; see [15]. This is the model dealt with in [22] and [4] (the last one with the simplification $a(x) = x$, $b(x) = 1$).

3. RESCALED EQUATION, AND ASYMPTOTIC PROFILES

In order to investigate the large time behavior, Lifshitz–Slyozov make use of a scaling involving the critical size in the definition of the new time and space variables. However, monotonicity of $t \mapsto c(t)$ is not guaranteed

at all (on the contrary, numerical simulations show that, especially at earlier stages, this function is not monotone, see [6] and Sec. 4), so that the change of variables in [18] does not clearly make sense. On the other hand, one expects that $c(t)$ behaves for large time as $Kt^{-1/3}$, thus the critical size $x_c(t)$ behaves as t/K^3. In fact, this result has been rigorously proved in certain cases in [23]. This behavior is revealed by the numerical simulations, as we shall see in next section. This motivates the introduction of the following scaling:

$$\begin{cases} f(t,x) = \dfrac{1}{(1+t)^2}\, g\left(\ln(1+t), \dfrac{x}{1+t}\right), \\ \tau = \ln(1+t), \qquad y = \dfrac{x}{1+t}. \end{cases}$$

Roughly speaking, we replace x_c in the scaling of [18] by the monotone function $(1+t)$. We set

$$d(\ln(1+t)) = (1+t)^{1/3}\, c(t), \qquad w(\tau, y) = y^{1/3} d(\tau) - 1 - y.$$

A short computation leads to the following rescaled form of (1.1)

$$\begin{cases} \dfrac{\partial g}{\partial \tau} + \dfrac{\partial}{\partial y}\left[w(\tau, y)\, g\right] = g, \\ d(\tau)\, e^{-\tau/3} + \displaystyle\int_{\mathbb{R}^+} y g(\tau, y)\, dy = \rho. \end{cases}$$

Based on the analysis of [18, 23], confirmed on this aspect by the numerical tests in Sec. 4, one expects that $c(t)\, t^{1/3}$ tends to some constant $K > 0$, i.e.,

$$\lim_{\tau \to \infty} d(\tau) = K.$$

Accordingly, $d(\tau)\, e^{-\tau/3} \sim K e^{-\tau/3}$ is negligible for large τ. Similarly, $w(\tau, y)$ looks like $w_K(y) = y^{1/3} K - 1 - y$. Thus, one is led to the following limit equation

$$\begin{cases} \dfrac{\partial g}{\partial \tau} + \dfrac{\partial}{\partial y}\left[w_K(y)\, g\right] = g, \\ \displaystyle\int_{\mathbb{R}^+} y g(\tau, y)\, dy = \rho \end{cases} \tag{3.1}$$

Notice that, from previous equation and the constraint on the first moment of g, K is equal to the inverse of the mean radius

$$K = \int_{\mathbb{R}^+} g\,dy \left(\int_{\mathbb{R}^+} y^{1/3} g\,dy \right)^{-1}.$$

To go further, one needs to discuss some basic properties of the asymptotic growth rate $w_K(y) = W_K(y^{1/3})$, where W_K is the simple polynomial $W_K(z) = Kz - 1 - z^3$. We shall obtain a family of possible asymptotic profiles, parameterized by K. We remark that W_K is concave on $(0, +\infty)$ and reaches its maximum at $z = \sqrt{K/3}$. We have, for $z \geqslant 0$,

$$W_K(z) \leqslant W_K^{\max} = K(K/3)^{1/2} - 1 - (K/3)^{3/2} = 2(K/3)^{3/2} - 1.$$

Next, remark that $W_K^{\max}$ is an increasing function of K, from $(0, +\infty)$ to $(-1, +\infty)$, which vanishes at the critical value

$$K_{\text{crit}} = 3/2^{2/3}.$$

Therefore, we distinguish three cases:

(a) $K < K_{\text{crit}}$: W_K has no positive roots, $W_K(z) \leqslant W_K^{\max} < 0$ for $z \geqslant 0$.

(b) $K > K_{\text{crit}}$: W_K has two distinct positive roots, z_0, z_+ (and a negative root z_-), and we have $W_K(z) \leqslant 0$ for $0 \leqslant z \leqslant z_0$ or $z \geqslant z_+$, and $W_K(z) \geqslant 0$ for $z_0 \leqslant z \leqslant z_+$. We will denote by y_-, y_+ and y_0 the corresponding values for $w_K(y)$, i.e., $y_i = z_i^3$ for $i \in \{-, 0, +\}$.

(c) $K = K_{\text{crit}}$: $\sqrt{K_{\text{crit}}/3} = 2^{-1/3}$ is a double root and $W_K(z) \leqslant 0$ for $z \geqslant 0$.

Let us now look at the stationary solution M_K of (3.1)

$$\partial_y (w_K(y)\, M_K) = M_K \qquad \text{for} \quad y \geqslant 0.$$

At least formally (up to the first positive zero $y_0 = z_0^3$ of w_K) we can write

$$M_K(y) = \frac{-1}{w_K(y)} \exp\left(\int_0^y \frac{d\sigma}{w_K(\sigma)} \right) = -\frac{d}{dy}\left[\exp\left(\int_0^y \frac{d\sigma}{w_K(\sigma)} \right) \right].$$

Furthermore, for such a solution to be admissible, it should satisfy the integrability condition $yM_K(y) \in L^1(\mathbb{R}^+)$.

We shall see that the sub-critical case is unphysical; while for $K \geqslant K_{\text{crit}}$, the value of K can be related, roughly speaking, to the behavior of the stationary solution at the end of its support. This proposition can be also found in [23].

Proposition 3.1. For $K < K_{\text{crit}}$, there is no admissible stationary solution. For $K = K_{\text{crit}}$, one obtains the Lifshitz–Slyozov profile

$$M_{\text{crit}}(y) = \frac{\exp\left(-\dfrac{(2y)^{1/3}}{1-(2y)^{1/3}}\right)}{(1-(2y)^{1/3})^{11/3}\,(1+\frac{1}{2}(2y)^{1/3})^{7/3}}, \tag{3.2}$$

for $0 \leqslant y \leqslant y_0 = 1/2$, and 0 otherwise. For $K > K_{\text{crit}}$, one has

$$M_K(y) = (y_0\, y_-\, y_+)^{1/3}\, \frac{(1-(y/y_0)^{1/3})^{p-1}}{(1-(y/y_-)^{1/3})^{1-q}\,(1-(y/y_+)^{1/3})^{1-r}}, \tag{3.3}$$

for $0 \leqslant y \leqslant y_0$, and 0 otherwise, where the exponents $p \geqslant 0$, q, r depend on K. In particular, p and K are related by

$$K = \frac{3(p+1)}{(2p+3)^{2/3}\, p^{1/3}}. \tag{3.4}$$

Proof. The integrability requirement excludes the sub-critical case $K < K_{\text{crit}}$: we shall show that the first moment blows up. Indeed, for $K < K_{\text{crit}}$, $\sigma \mapsto w_K(\sigma)^{-1}$ is defined on the whole interval $(0, +\infty)$, and we remark that, for any $y \geqslant 0$,

$$\begin{aligned}(1+y)\exp\left(\int_0^y \frac{d\sigma}{w_K(\sigma)}\right) &= \exp\left(\int_0^y \frac{d\sigma}{w_K(\sigma)} + \int_0^y \frac{d\sigma}{1+\sigma}\right)\\ &= \exp\left(\int_0^y \frac{K\sigma^{1/3}\, d\sigma}{(1+\sigma)(K\sigma^{1/3}-1-\sigma)}\right).\end{aligned}$$

The integrand is non positive and behaves for large σ's as $-K\sigma^{-5/3}$ which is integrable at infinity. It follows that

$$\lim_{y\to\infty} (1+y)\exp\left(\int_0^y \frac{d\sigma}{w_K(\sigma)}\right) = \ell > 0.$$

In particular, for $y \geqslant Y$ large enough, we have $(1+y)\exp(\int_0^y \frac{d\sigma}{w_K(\sigma)}) \geqslant \ell/2 > 0$. Since $-y/w_K(y) \to 1$ as $y \to \infty$, we deduce that

$$yM_K(y) = \frac{y}{-w_K(y)}(1+y)\exp\left(\int_0^y \frac{d\sigma}{w_K(\sigma)}\right)\frac{1}{1+y} \geqslant \frac{\ell}{4}\frac{1}{1+y},$$

holds for $y \geqslant Y$ large enough. Consequently $yM_K(y) \notin L^1(\mathbb{R}^+)$ for $K < K_{\text{crit}}$. Lifshitz–Slyozov also exclude in their analysis the case $K > K_{\text{crit}}$; however,

this is far from clear, in particular when dealing with compactly supported initial data, see [4, 19, 22, 23].

Let us now look at the critical case $K = K_{\text{crit}} = 3/2^{2/3}$. We can rewrite $W_{K_{\text{crit}}}(z) = -(z-2^{-1/3})^2\,(z+2^{2/3})$. Accordingly, we get for $0 \leqslant y \leqslant 1/2$

$$\begin{aligned}\int_0^y \frac{d\sigma}{w_{K_{\text{crit}}}(\sigma)} &= \int_0^{y^{1/3}} \frac{3z^2\,dz}{W_{K_{\text{crit}}}(z)}\\ &= \int_0^{y^{1/3}} \left(\frac{-5/3}{z-2^{-1/3}} - \frac{2^{-1/3}}{(z-2^{-1/3})^2} - \frac{4/3}{z+2^{2/3}}\right) dz\\ &= 1 + \frac{1}{(2y)^{1/3}-1} + \ln\left(\frac{(1-(2y)^{1/3})^{-5/3}}{(1+(y/4)^{1/3})^{4/3}}\right),\end{aligned}$$

which yields the announced formula (3.2) for $0 \leqslant y \leqslant y_0 = 1/2$.

We turn to the supercritical case $K > K_{\text{crit}}$. The polynomial W_K has three distinct roots denoted by

$$z_- < 0 < z_0 < \sqrt{K/3} < z_+.$$

Let us write $z_\pm$ in terms of the first positive root z_0 as follows

$$\begin{cases} -W_K(z) = (z-z_0)(z^2+z_0 z-(K-z_0^2)) = (z-z_0)(z-z_+)(z-z_-)\\ z_\pm = \frac{1}{2}(-z_0 \pm \sqrt{4K-3z_0^2}).\end{cases}$$

We aim at computing

$$\begin{aligned}\int_0^y \frac{d\sigma}{w_K(\sigma)} &= \int_0^{y^{1/3}} \frac{-3z^2\,dz}{(z-z_0)(z-z_+)(z-z_-)}\\ &= \int_0^{y^{1/3}} \left(\frac{p}{z-z_0} + \frac{q}{z-z_-} + \frac{r}{z-z_+}\right) dz\end{aligned}$$

where we check that

$$p = \frac{3z_0^2}{(z_0-z_-)(z_+-z_0)}, \qquad q = \frac{-3z_-^2}{(z_0-z_-)(z_+-z_-)}$$

and

$$r = \frac{-3z_+^2}{(z_+-z_0)(z_+-z_-)}.$$

For convenience, let us set

$$\kappa = \frac{K}{3z_0^2} \geqslant 1, \qquad \alpha = \frac{1}{2}(-1+\sqrt{3}\sqrt{4\kappa-1}),$$

so that

$$z_+ = \alpha z_0, \qquad z_- = -z_0 - z_+ = -z_0(1+\alpha),$$

and

$$p = \frac{3}{(2+\alpha)(\alpha-1)} = \frac{1}{\kappa-1} \geqslant 1, \qquad q = \frac{-3(\alpha+1)^2}{(2\alpha+1)(\alpha+2)}$$

and

$$r = \frac{-3\alpha^2}{(\alpha-1)(2\alpha+1)}.$$

Hence, we get

$$\int_0^y \frac{d\sigma}{w_K(\sigma)} = \ln\{(1-(y/y_0)^{1/3})^p\,(1-(y/y_-)^{1/3})^q\,(1-(y/y_+)^{1/3})^r\}$$

which yields the announced formula (3.3).

The behavior at the endpoint y_0 is determined by the exponent $p-1$. Recall this quantity is related to the value of

$$K = \lim_{t\to\infty} c(t)\,t^{1/3} = \lim_{\tau\to\infty} d(\tau)$$

by the relation

$$p = \frac{1}{\kappa-1}, \qquad \kappa = \frac{K}{3z_0^2}$$

where z_0 is the first positive root of W_K i.e., $W_K(z_0) = 0 = Kz_0 - 1 - z_0^3$. This allows us to express K as a function of the exponent p as in the relation (3.4).

For $K \geqslant K_{\text{crit}}$, we have computed the stationary solution M_K up to the first positive root y_0 of w_K, where it vanishes. It remains to check that the integrability condition implies that M_K should be extended by 0 for $y \geqslant y_0$.

Note that M_{crit} is C^∞ at the tip of its support y_0, while the stationary solutions M_K are less regular as K increases, i.e., p tends to 0 (see Fig. 1 for a comparison of the graphs). □

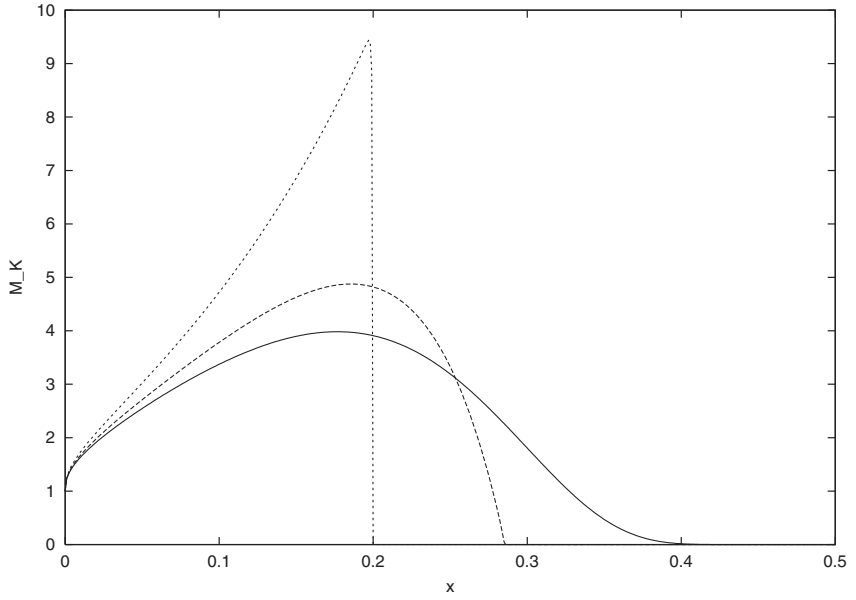

Fig. 1. Comparisons of the stationary solutions M_K profiles for the discontinuous case $p=1$, the corner case $p=2$ and the smooth case $p=\infty$ (LS profile).

Remark 3.2. For $p>2$, M_K and M'_K vanish at the end of their support. For $p=2$, M_K vanishes but M'_K is a negative constant as $y \to y_0^-$ (it behaves like a triangle function). For $1<p<2$, M_K vanishes and M'_K blows up as $y \to y_0^-$. For $p=1$, M_K behaves like a step function. For $0<p<1$, M_K and M'_K blow up as $y \to y_0^-$ with an integrable singularity. For $p \to 0$, M_K looks like a Dirac function at y_0.

Let us go back to the rescaled equation (3.1) when d has reached its equilibrium value. Set $g(\tau, y) = h(\tau, y)\, M_K(y)$. It follows that

$$\partial_\tau h + w_K(y)\, \partial_y h = 0.$$

Hence, integrating along the associated characteristics, we can write

$$h(\tau, y) = \chi(\tau - \Phi_K(y)), \qquad \Phi_K(y) = \int_0^y \frac{d\sigma}{w_K(\sigma)}.$$

Furthermore, the mass conservation yields

$$\int_{\mathbb{R}^+} y h(\tau, y)\, M_K(y)\, dy = \rho = \int_{\mathbb{R}^+} y \chi(\tau - \Phi_K(y))\, M_K(y)\, dy.$$

With the change of variables $z = \tau - \Phi_K(y) \geqslant 0$, this can be rewritten as

$$\rho = \int_\tau^\infty \Phi_K^{-1}(\tau - z)\, e^{\tau - z} \chi(z)\, dz,$$

where $\Phi_K^{-1}: (-\infty, 0] \to [0, y_0)$ is the inverse of the decreasing function $\Phi_K: [0, y_0) \to (-\infty, 0]$. An obvious solution of this equation is given by $\chi(y) = A$ constant, determined by the relation

$$A = \rho \left(\int_{\mathbb{R}^+} y M_K(y)\, dy \right)^{-1}.$$

It yields

$$f(t, x) = \frac{1}{(1+t)^2}\, g\left(\ln(1+t), \frac{x}{1+t} \right) \sim \frac{A}{(1+t)^2}\, M_K\left(\frac{x}{1+t} \right)$$

for large time. The zeroth order moment of f, i.e., the total number of clusters, behaves as

$$m_0(t) = \int_{\mathbb{R}^+} f(t, x)\, dx \sim \frac{A}{1+t} \int_{\mathbb{R}^+} M_K\left(\frac{x}{1+t} \right) \frac{dx}{1+t} \sim \frac{A}{t} \int_{\mathbb{R}^+} M_K(y)\, dy.$$

In view of the discussion above and the results obtained in [19, 4, 22, 23] one might expect the following conjecture for the LS system. If the initial data is compactly supported in $[0, x_s]$, with $f_0(x) \sim C(x_s - x)^{p-1}$ when $x \to x_s^-$, then the solution satisfies

$$f(t, x) \sim \frac{A}{(1+t)^2}\, M_K\left(\frac{x}{1+t} \right) \tag{3.5}$$

where K is associated to p by (3.4). If f_0 has unbounded support, the conjecture is

$$f(t, x) \sim \frac{A}{(1+t)^2}\, M_{\text{crit}}\left(\frac{x}{1+t} \right), \tag{3.6}$$

i.e., f is described by the LS profile. This conjecture implies that CLS2 and CLS3 hold with the corresponding value for K. We recall that this behavior has been proved for "small" values of the exponent p. For p small enough and an initial data close to the equilibrium state associated to that p, the

condition that the initial data is "regularly varying with exponent p" is necessary and sufficient to have convergence to the asymptotic profile as time goes to infinity. For general p the condition has only been shown to be necessary. We refer for precise definition and details to the paper [22, 23]. Also, the description of the family of stationary solutions and the different asymptotic profiles are described in [23].

4. NUMERICAL SIMULATION OF LS

We wish to numerically investigate the question of the asymptotic behavior of solutions of (1.1). We have seen the possibility of having different asymptotic states depending on the behavior near the tip of the support in previous section. This is the main point we would like to validate and obtain numerically. On the other hand, we want to verify the possibility of convergence towards the smooth LS profile for non compactly supported or positive fast decaying at infinity initial data.

Is the smooth stationary state M_{crit} the universal long-time profile for the LS system? Are there any other initial data that leads to the non-smooth self similar profiles M_K for $K > K_{\text{crit}}$? The LS conjecture CLS4 asserts that the answer to the first question is affirmative. However, we will show by a carefully constructed numerical scheme that in fact, the second answer is affirmative and the LS conjecture CLS4 in its full generality is not true.

Concerning the smooth LS profile, does the evolution lead positive or compactly supported initial data towards the smooth LS profile? How large is the asymptotic stability neighborhoods for M_{crit}? We will present evolution results for several initial data leading to the smooth profile with monotonic tails. However, as shown by a counterexample in [4], we can imagine that oscillations in the tail of the initial distribution can prevent us from convergence to the smooth asymptotic profile. We show results for more aggressive initial data with non monotonic tail, see Figs. 26 and 27. The results reinforce the conjecture that under suitable additional assumptions on positive initial data, like having Gaussian tail at ∞, the solution converges towards the smooth LS profile. This is a very interesting open problem.

The rigorous proof of part of these results was achieved in [22, 23] but a complete understanding is still lacking, mainly for non compactly supported initial data. The proposed method is a scheme for the LS system that differentiates among the asymptotic profiles, as we shall see. Let us point out that the complexity and great sensitivity of the LS system shown by [23] is a very difficult and challenging problem to be numerically resolved.

This section is divided into two subsections: in the first one we describe the numerical scheme used to discretize (1.1), the second one is devoted to the numerical simulation results in which previous assertions are based on and their discussion.

4.1. Numerical Method

We treat the evolution equation

$$\frac{\partial f}{\partial t}+\frac{\partial}{\partial x}\left[V(t, x)\, f\right]=0 \tag{4.1}$$

as a linear one-dimensional advection equation with time and position dependent advection function $V(t, x)=a(x)\, c(t)-b(x)$, for a given known monomer concentration $c(t)$. In order to solve numerically such linear advection equation we can use any standard numerical scheme [16, 27] considered for nonlinear conservation laws. In order to choose a suitable scheme for solving (4.1), we have to take into consideration several facts:

1. One of the effects over the solution we observe is the stretching of the support of the solution. Thus, one needs to deal with a large domain of computation.
2. The expected asymptotic profile depends crucially on the behavior of the data at the end of the support; therefore, smoothing effects induced by the numerical scheme can modify the final profile. As a consequence, one should choose the least dissipative choice among all the possible numerical schemes. Intuitively, the LS evolution acts in this way: zoom the tip of the support, cut the rest, stretch it and multiply locally by an amplification factor. Thus, smoothing effects done by the numerical approximations are doomed to be amplified during the evolution. This is the main reason we need the least possible dissipative numerical scheme.
3. High order accuracy for the solution in space is desirable since we expect the solution to be very smooth outside possibly the tip of the support. If we have initial solutions with jumps or corner discontinuities at the tip of the support, we expect them to propagate in time, so we would also need a numerical scheme that resolves shocks or corner discontinuities with a good accuracy, if they appear (see Figs. 1 and 2).
4. High order in time, TVD discretizations and stability in time are of paramount importance to obtain meaningful numerical results after so many time iterations.

Based on these facts, we decide to choose a standard finite volume solver of the linear advection equation (4.1) with Godunov flux as monotone flux. The choice of Godunov flux is due to the fact that is the least dissipative (less smearing of jumps or corners) with respect to other standard fluxes: Lax–Friedrichs, Engquist–Osher,... .

In the reconstruction part we want to achieve high order in smooth parts of the solution (that for (1.1) is always the case except possibly at the tip of the support) and also good accuracy at shocks (jumps) or corners, if they initially appear. Therefore, we choose WENO reconstruction with 5 points which gives us fifth-order spatial accuracy for smooth solutions. We refer to [13, 27] for the details of the numerical method. This method has been tested thoroughly and it has been shown to be very robust and to produce meaningful results for complicated non linear systems of conservation laws in fluid dynamics, semiconductors, Hamilton–Jacobi equations,... (see [27] and references therein).

We solve in time by means of an explicit 3rd-order TVD Runge–Kutta method [26] that enjoys the needed features of stability, high order and TVD character. CFL condition is verified at each time step to ensure numerical stability. The algebraic condition

$$c(t)+\int_{\mathbb{R}^+} xf(t,x)\,dx=\rho>0,$$

is used to determine the monomer concentration $c(t)$ at each evaluation needed in the Runge–Kutta method to compute the fluxes correctly.

In Fig. 2 we show the solution of this system for a step-like initial data after 200 units of time by using the finite volume Godunov-WENO, finite volume Lax–Friedrichs-WENO and the simple up-winding finite differences method (finite volume Godunov-first order reconstruction). We have solved the LS system with the different methods over the interval [0, 800] with 100 cells per unit length. Experts in numerical schemes for conservation laws can recognize easily that the simple up-winding method gives very smeared non realistic solutions for the linear advection equation with a step function as an initial data [16].

In fact the results of simulations for this system using the up-winding method were reported in [6]. They asserted that the LS conjecture was true by using different shapes of initial data, all of them with empty zero level set (non compact support). The smearing caused by the use of the simple up-winding method disables the possibility of finding any other possible behavior. In fact, as Fig. 2 shows, the use of this method for a step-like initial data can lead you to a completely wrong conclusion asserting the convergence towards the smooth self similar solution and therefore that the

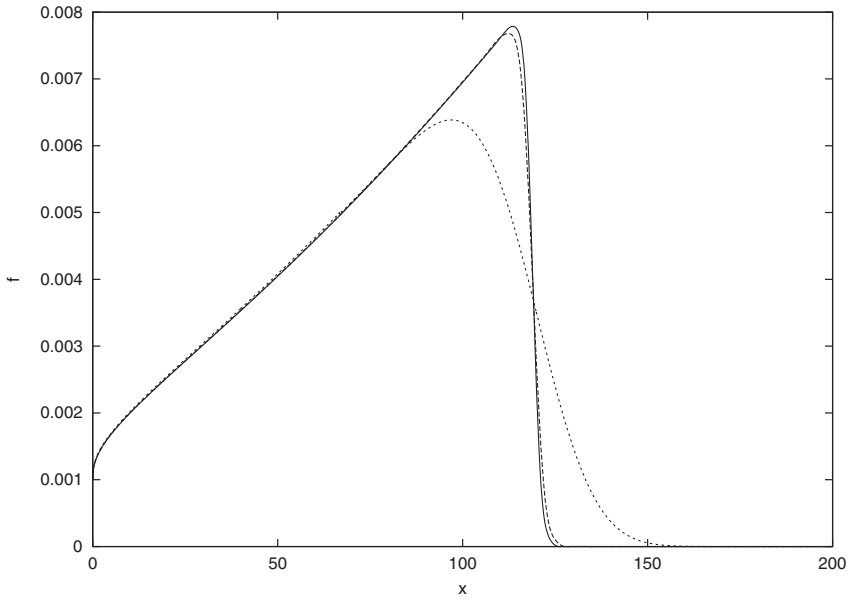

Fig. 2. Comparisons of the numerical solutions for a step-like function initial data ($f_0 = 0.1$ for $10 \leqslant x \leqslant 30$ and 0 outside) using finite volume Godunov-WENO, finite volume Lax–Friedrichs-WENO and upwinding finite difference method. The results given by Godunov-WENO are the least smeared, the upwinding results are the smoother ones.

LS profile is the universal asymptotic behavior for any initial data. This method is not at all suitable for controlling the behavior at the tip of the support. Moreover, they obtain limiting critical values K_{crit} with a error of 5–20%.

Being in principle such a simple looking numerical problem: a one dimensional advection equation coupled with an algebraic constraint, one has different choices for the numerical method. The objective of this paper is not to compare different numerical methods, their efficiency and their performance applied to the LS system and rather to highlight some of the open questions on the LS system using a suitable numerical method. We comment on other possible approaches, although in any case we want to include a detailed comparison of them.

One possibility would be to solve the characteristic system (1.2) in each time step by a suitable ODE solver and propagate the initial data through the characteristics by (2.1) together with the computation of the monomer concentration. The main disadvantage of these approaches is that many points will leave the computational domain from the left (those corresponding to small values of the size) and thus, one is forced to introduce

new points every certain number of time iterations. This fact produces a new source of numerical error since typically these new points will be included by some interpolation procedure and it might be that the resolution at the tip of the support is deteriorated.

Of course, other high order methods different from WENO should produce similar results for the case of smooth profiles and even for the non smooth case if they are capable of dealing with the numerical difficulties concerning non smooth profiles (see again the comparison in Fig. 2). For the Maxwellian initial data, any naive implementation of the method of lines using simple central finite differences and explicit 4th order Runge–Kutta method gives the same results but it does not for the non smooth initial data. The difficulty of the numerical challenge is illustrated also by Filbet and Laurençot [12] who introduced a time explicit finite volume numerical scheme, adapted for LS: the scheme is shown to be convergent, however it introduces too much diffusive effects to capture non smooth large time behavior.

Finally, let just mention that the numerical simulation of the rescaled equation

$$\begin{cases} \partial_\tau g + \partial_y (w(\tau, y)\, g) = g, \\ d(\tau)\, e^{-\tau/3} + \int_{\mathbb{R}^+} y g(\tau, y)\, dy = \rho. \end{cases}$$

is done following the same lines as above. Since we are applying the method of lines, the right-hand side is explicitly included as a part of the function defining the ODE system solved by the above mentioned Runge–Kutta method. The main advantage of this rescaled form is that we can work in a much smaller x-interval. Despite this fact, the CFL condition for the rescaled equation is much more restrictive (stiffer problem) than for the original LS system. Therefore, computational times are almost identical for both problems, but the rescaled system allows us to explore easier the later stages of the evolution. The use of certain numerical methods especially designed to treat stiff problems (see [28]) should be explored for solving the rescaled LS system. Also, the modified LSW system is solved in an analogous way to the LS system.

4.2. Simulation Results

4.2.1. Validation of the Code

First, we validate our code by comparing simulation results to explicit solutions. Explicit solutions were obtained in [7] for very simple coefficients

without critical size. In particular, the simplest case is $a(x) = ax$, $b(x) = bx$, with $a, b > 0$ constants, where the solution is exactly known

$$f(t, x) = \beta(t)\, f_0(\beta(t)\, x),$$

with

$$\beta(t) = \begin{cases} \dfrac{(ac_0 - b)\exp((b - a\rho)\, t) + a(\rho - c_0)}{a\rho - b}, & \text{for} \quad a\rho - b \neq 0, \\ \beta(t) = 1 + a(\rho - c_0)\, t, & \text{for} \quad a\rho - b = 0, \end{cases}$$

whereas

$$c(t) = \begin{cases} \dfrac{\rho(ac_0 - b)\exp((b - a\rho)\, t) + b(\rho - c_0)}{(ac_0 - b)\exp((b - a\rho)\, t) + a(\rho - c_0)}, & \text{for} \quad a\rho - b \neq 0, \\ \dfrac{c_0 + \rho(\rho - c_0)\, at}{1 + (\rho - c_0)\, at}, & \text{for} \quad a\rho - b = 0, \end{cases}$$

Then, the asymptotic behavior is obtained easily, depending on the over or undersatured nature of the initial data. Precisely, one has:

If $\rho < b/a$, then $c(t) \to \rho$ and

$$f(t, x) \sim \frac{b/a - c_0}{b/a - \rho}\, e^{(b/a - \rho)\, at} f_0\left(\frac{b/a - c_0}{b/a - \rho}\, e^{(b/a - \rho)\, at}\, x\right),$$

If $\rho > b/a$, then $c(t) \to b/a$ and

$$f(t, x) \to f_\infty(x) = \frac{\rho - c_0}{\rho - b/a}\, f_0\left(\frac{\rho - c_0}{\rho - b/a}\, x\right).$$

We use this simple case to validate the performance of the scheme. The first test (Test 1) corresponds to $a = b = 1$, $\rho = 41 > b/a$, $c_0 = 31$. The initial data, represented in Fig. 3 bottom right, is a Maxwellian

$$f_0(x) = \frac{m}{\sqrt{2\pi}} \exp\left(-\frac{(x - 10)^2}{2}\right).$$

Figure 3 shows an exact agreement of the computed solution with the exact behavior given by

$$c(t) = \frac{40 \times 30 \times e^{-40t} + 10}{30 \times e^{-40t} + 10} \to 1 = b/a,$$

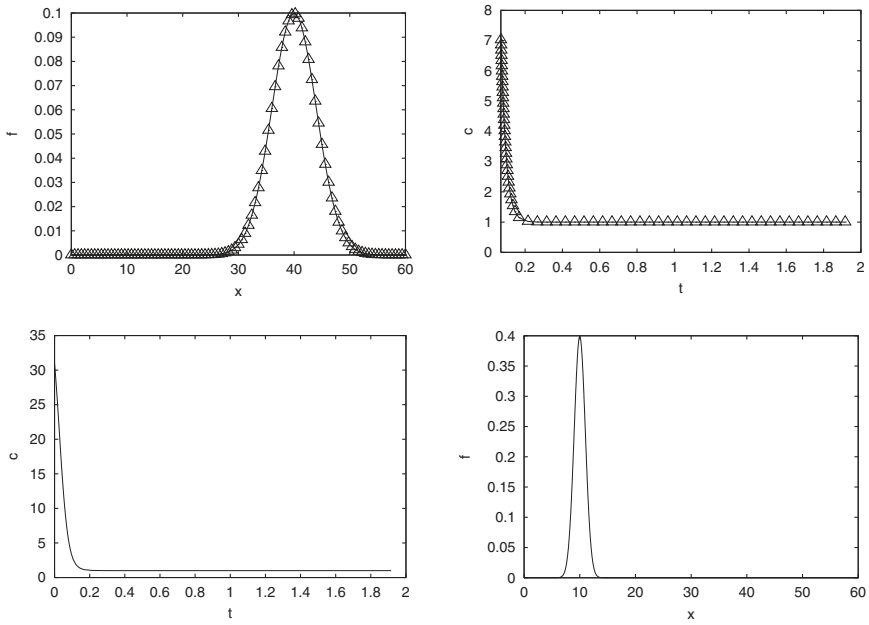

Fig. 3. Test1: top left: final computed solution (solid line) versus exact explicit stationary (triangles); top right: $c(t)$ for the computed solution (solid line) versus the exact explicit evolution of concentration of monomers (triangles); bottom left: $c(t)$; bottom right: initial data.

and $f(t, x) \sim \frac{1}{4} f_0(\frac{x}{4})$ as $t \to \infty$. The second test (Test 2) is $a = b = 1$, $\rho = 0.5 < b/a$, $c_0 \ll 1$ for which we recover the expected behavior $c(t) \sim 0.5$ and

$$f(t, x) \sim 2e^{t/2} f_0(e^{t/2}x) \sim \frac{2m}{\sqrt{2\pi e^{-t}}} \exp\left(-\frac{(x - 10e^{-t/2})^2}{2e^{-t}}\right) \sim 2m\delta_{x=0},$$

as $t \to \infty$. The monomer concentration evolution is given in Fig. 4.

Let us mention that we will show numerically converged results as we have validated the results for the LS system by mesh refinement study for several initial data (particularly a Maxwellian and a step function). All the results in this subsection have been obtained by solving the corresponding LS system over the interval [0, 60] with 30 cells per unit length.

4.2.2. Simulations on the LS Equation

Once we have validated our code we take the true LS system with the coefficients of [18], $a(x) = x^{1/3}$, $b(x) = 1$. We first, choose as initial data f_0

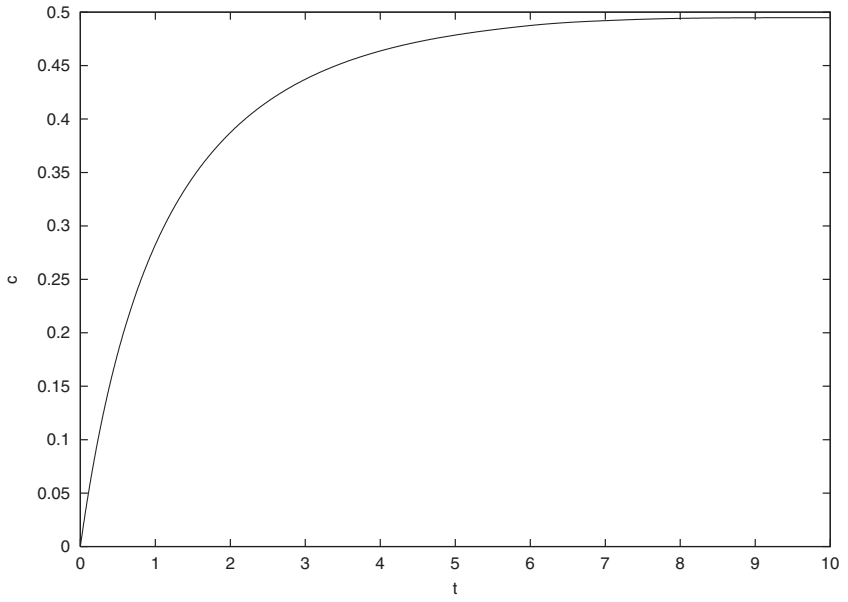

Fig. 4. Test 2: $c(t)$ for the computed solution.

a Maxwellian centered on x_0 comparable to, or larger than, the critical size. This is the situation in Theorem 1 [10] where $c(t)$ goes to 0 as $t \to \infty$. Precisely, we set for this run: $\rho = 41$, $c_0 = 1$ (thus $x_{c_0} = 1$) and the Maxwellian

$$f_0(x) = \frac{m}{\sqrt{2\pi}} \exp\left(-\frac{(x-10)^2}{2}\right).$$

as initial data (see Fig. 3 bottom right). We solve the LS system over the interval [0, 1000] with 40 cells per unit length.

After 2000 units of time, one observes (see Figs. 5 and 6):

1. A metastability region ($t < 50$) for the concentration of monomers before $c(t)$ decreases.
2. A good agreement with the $t^{-1/3}$ law, as shown in the graph of $K(t) = t^{1/3}c(t)$. We can observe that it converges very quickly towards values very close to $K_{\text{crit}} = 1.88988$, and after $K(t)$ changes very slowly decreasing their value until reaching $K(2000) = 1.8657$. We may run the code further to observe that thereafter $K(t)$ starts to increase slowly approaching the critical value $K_{\text{crit}} = 1.88988$, but we will see this fact later in the rescaled equation.

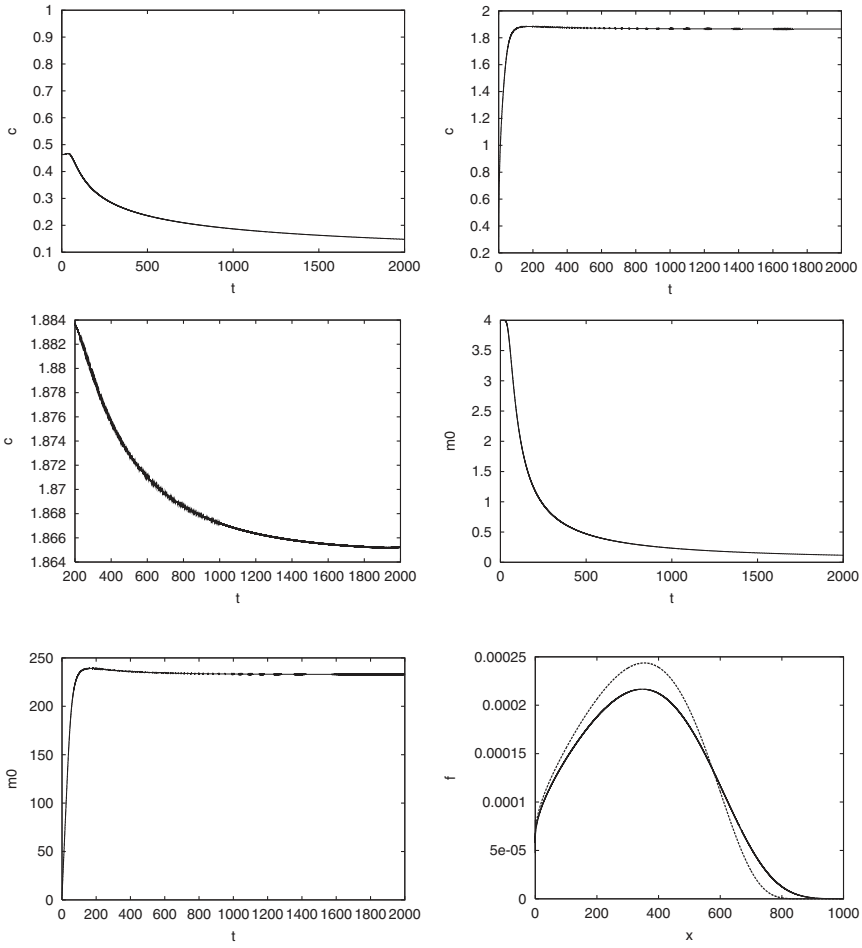

Fig. 5. Maxwellian initial data for the LS system ($c(t) \to 0$): top left: $c(t)$; top right: $t^{1/3}c(t)$; middle left: zoom of $t^{1/3}c(t)$; middle right: $m_0(t)$; bottom left: $tm_0(t)$; bottom right: final result (solid line) versus the corresponding LS profile (thicker solid line).

3. m_0 decreases after the metastability region, in good agreement with the t^{-1} law.
4. The evolution of this solution is summarized in Fig. 6 which shows the solution $f(t, x)$ each 250 units of time. We can see clearly the stretching of the support and the convergence towards the shape of the LS profile. In Fig. 5 bottom right we have plotted the final solution after 2000 units of time versus the LS profile in

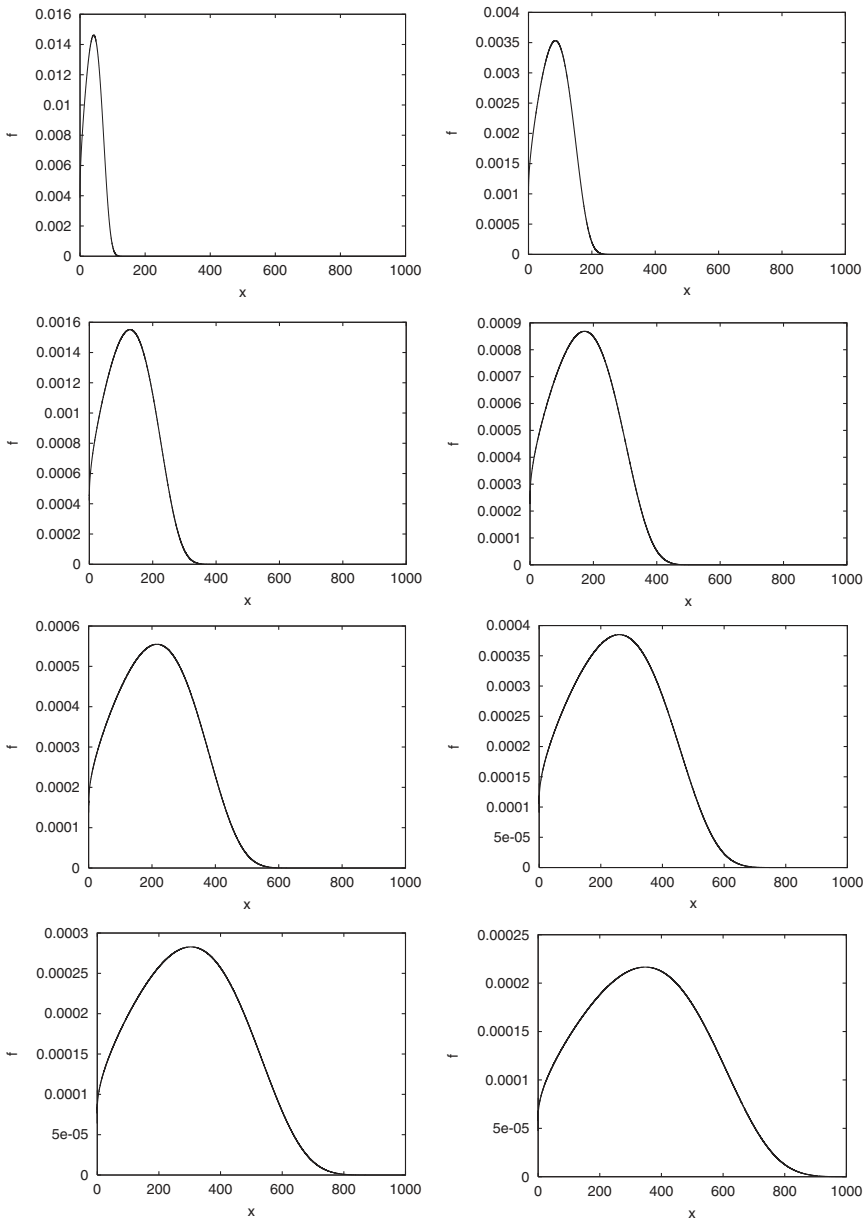

Fig. 6. Evolution of the Maxwellian initial data (see Fig. 3 bottom right) for the LS system every 250 time units.

the self similar variables corresponding to this time and to this value of ρ according to formula (3.6).

Next, we choose a very small c_0, thus a very large critical size. The initial data f_0 is a Maxwellian centered on x_0 much smaller than the critical size, with a small variance, so that it is almost a compactly supported data, with support to the left of the critical size. Then, one verifies that c goes to ρ. This is illustrated with the data: $c_0 = 7.10^{-2}$, $\rho = 0.2$ and f_0 is a Maxwellian centered at 0, with mass .1 and variance 10, given in Fig. 7 top left. After 45 units of time, one sees that c goes very close to ρ (see Fig. 7 top right) and the final profile $f(t, x)$ is almost zero (see Fig. 7 bottom). We solve the LS system over the interval $[0, 1000]$ with 40 cells per unit length.

However, this behavior is very sensitive to the initial data, it changes drastically if the initial critical size is reduced or if one increases the "support" of f_0 (for instance, changing the variance of the Maxwellian). We consider the same test as before changing $c_0 = 0.5$, $\rho = 2$, variance of f_0 equals 0.01 (see Fig. 8 top left). Then, c starts increasing, reaching values very close to ρ, but the evolution changes and finally it decreases to 0, as illustrated by Fig. 8 top right. We then recover a good agreement again

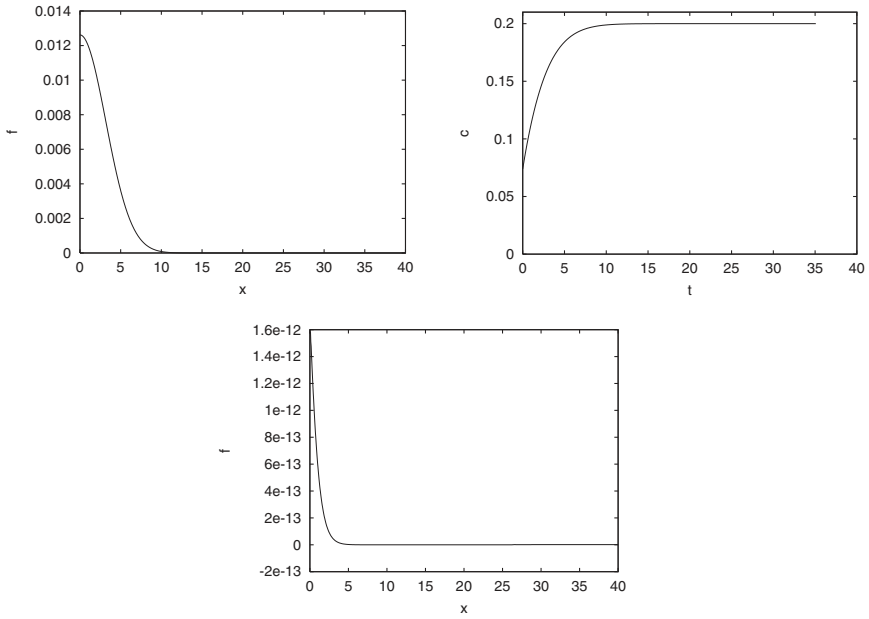

Fig. 7. Maxwellian initial data for the LS system ($c(t) \to \rho$): top left: initial data; top right: $c(t)$; bottom: final result.

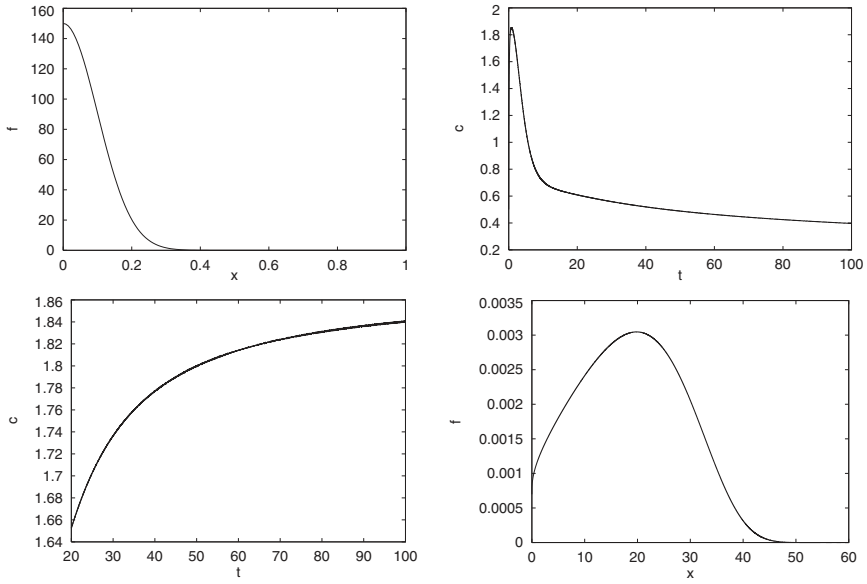

Fig. 8. Maxwellian initial data for the LS system ($c(t) \to 0$): top left: initial data; top right: $c(t)$; bottom left: $t^{1/3}c(t)$; bottom right: final result.

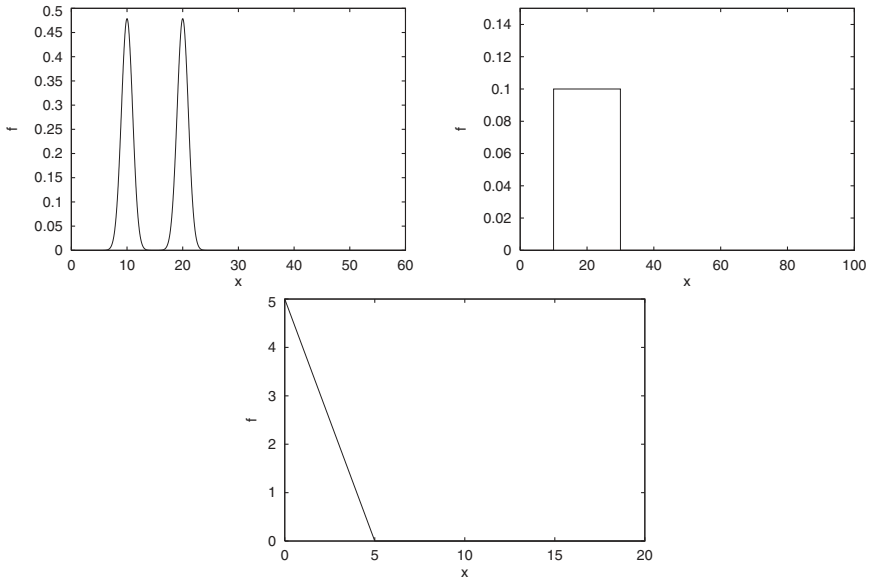

Fig. 9. Initial data for the LS system: top left: double Maxwellian; top right: step function; bottom: triangle function.

with the $t^{-1/3}$ law, see Fig. 8 bottom left. Figure 8 bottom right gives the final solution f, after 100 units of time.

Now, we want to check the LS conjecture about the universal asymptotic profile. In order to do this, we take three different initial data (see Fig. 9): another smooth non compactly supported initial data: the sum of 2 Maxwellians (we have also tested initial data with unbounded support and algebraic decay); a discontinuous compactly supported initial data: a step

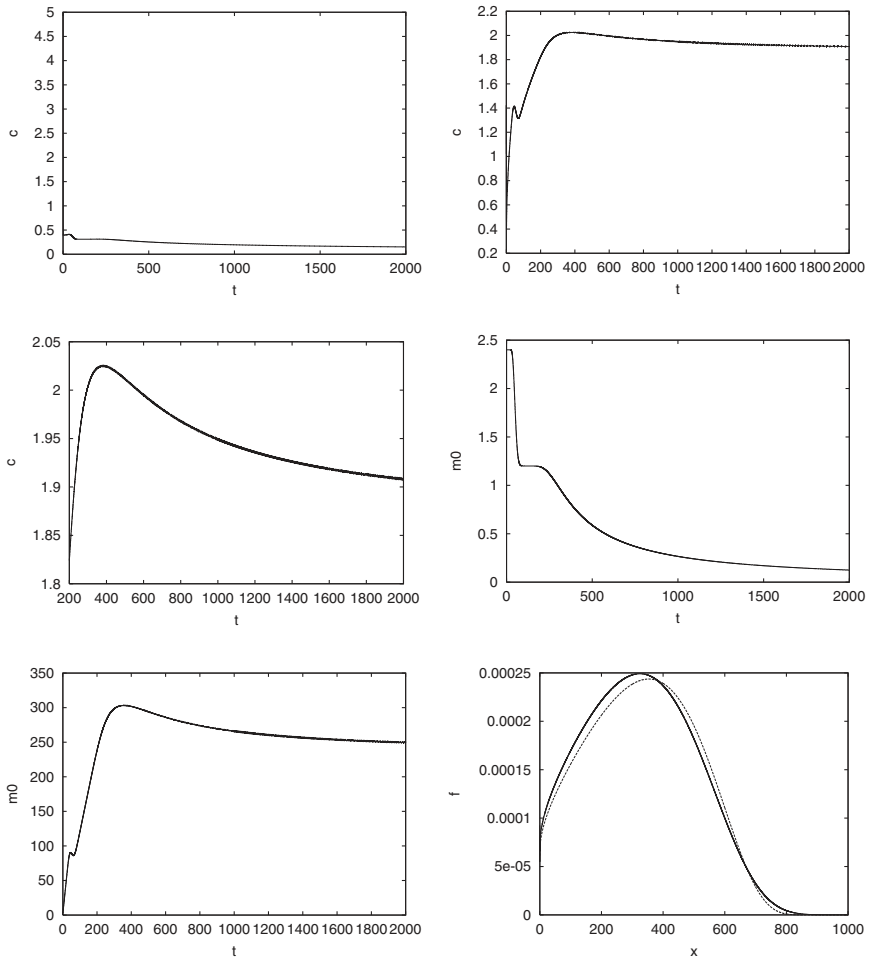

Fig. 10. Double Maxwellian initial data for the LS system: top left: $c(t)$; top right: $t^{1/3}c(t)$; middle left: zoom of $t^{1/3}c(t)$; middle right: $m_0(t)$; bottom left: $tm_0(t)$; bottom right: final result (solid line) versus the corresponding LS profile (thicker solid line).

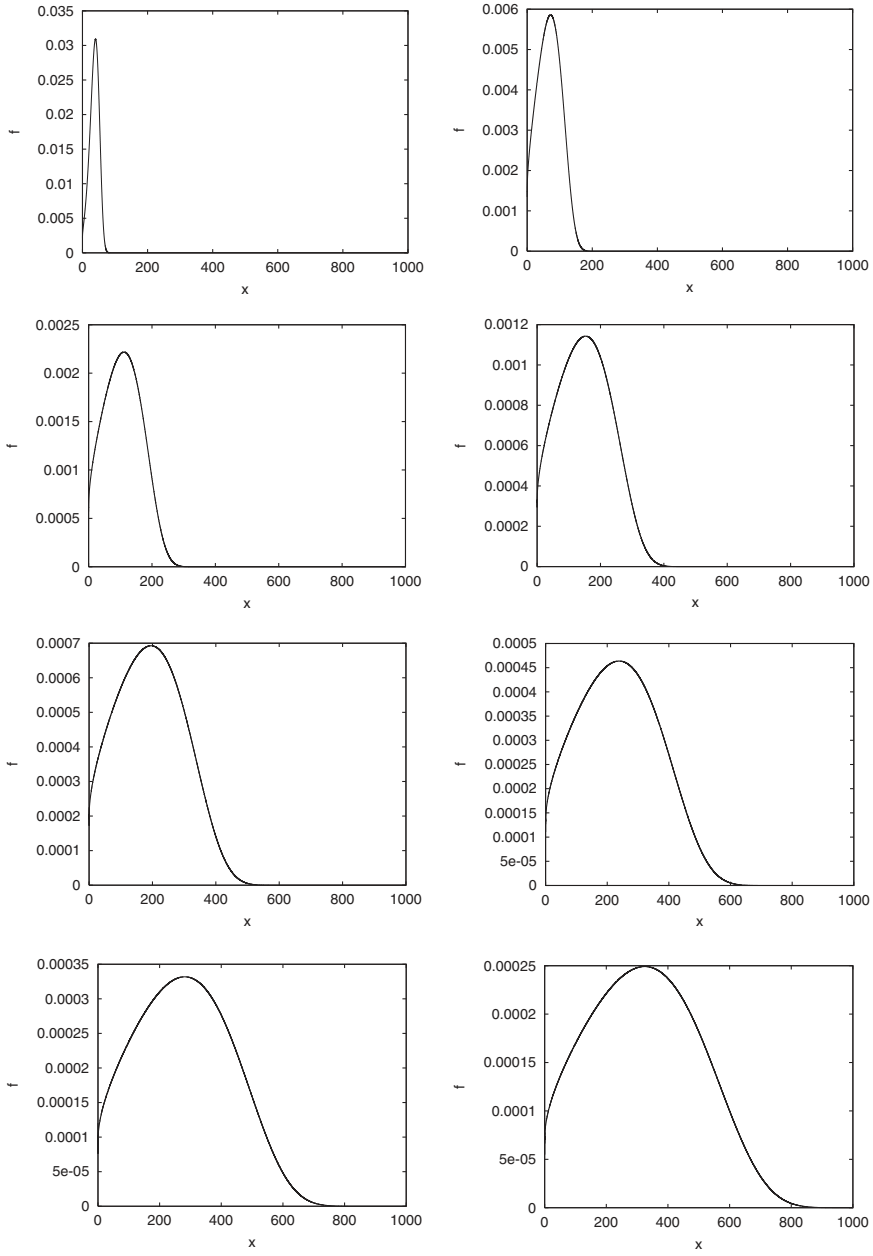

Fig. 11. Evolution of the double Maxwellian initial data for the LS system every 250 time units.

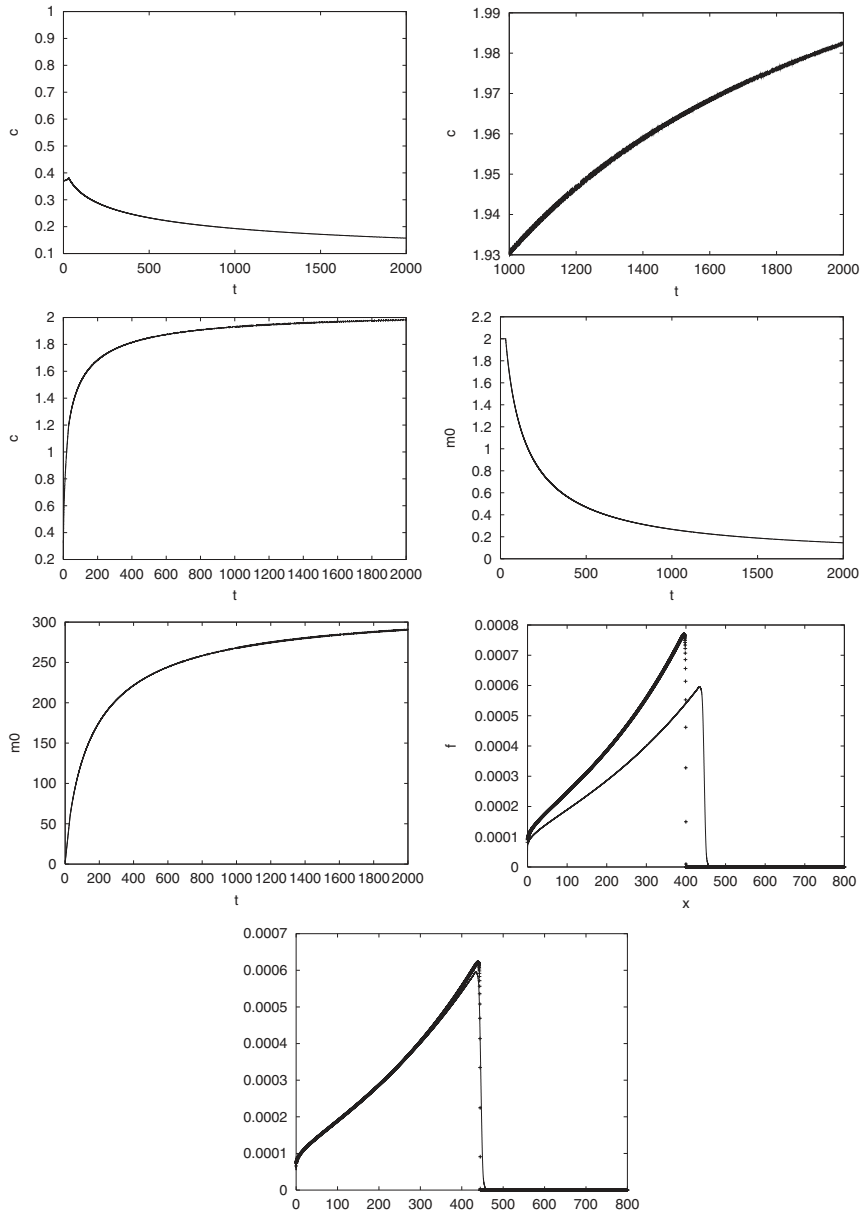

Fig. 12. Step function initial data for the LS system: top left: $c(t)$; top right: $t^{1/3}c(t)$; top middle left: zoom of $t^{1/3}c(t)$; top middle right: $m_0(t)$; bottom middle left: $tm_0(t)$; bottom middle right and bottom: final result (solid line) compared to LS profile (crosses) for two different time delays.

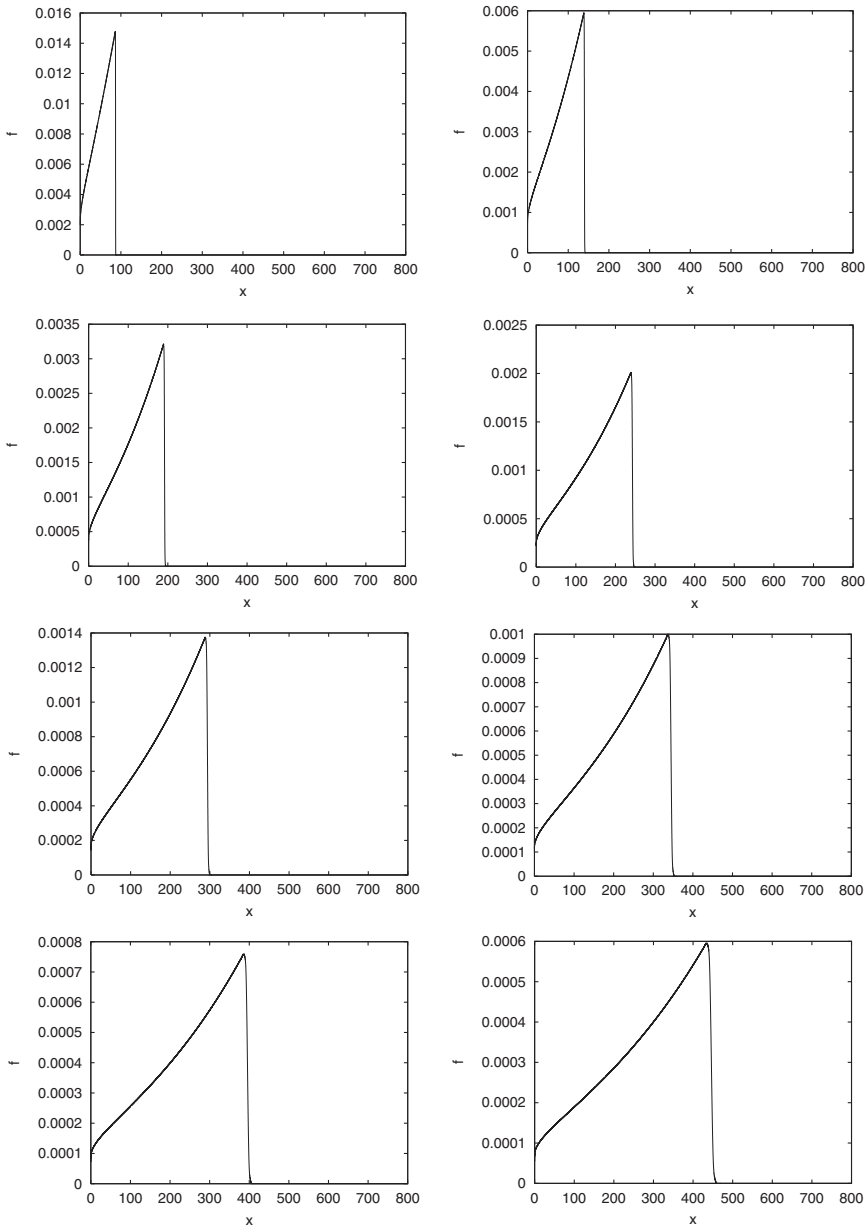

Fig. 13. Evolution of the step function initial data for the LS system every 250 time units.

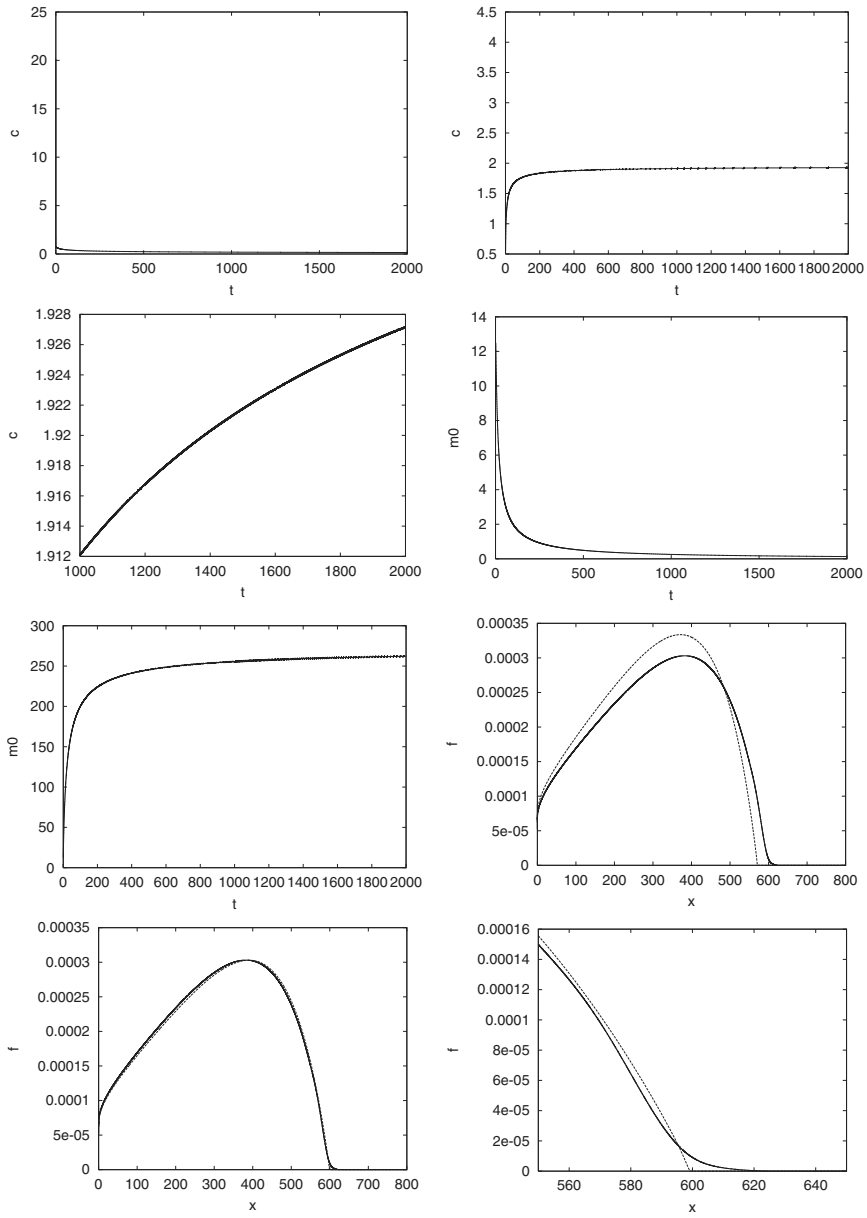

Fig. 14. Triangle function initial data for the LS system: top left: $c(t)$; top right: $t^{1/3}c(t)$; top middle left: zoom of $t^{1/3}c(t)$; top middle right: $m_0(t)$; bottom middle left: $tm_0(t)$; bottom middle right and bottom: final result (solid line) compared to LS (thicker line) for two different time delays.

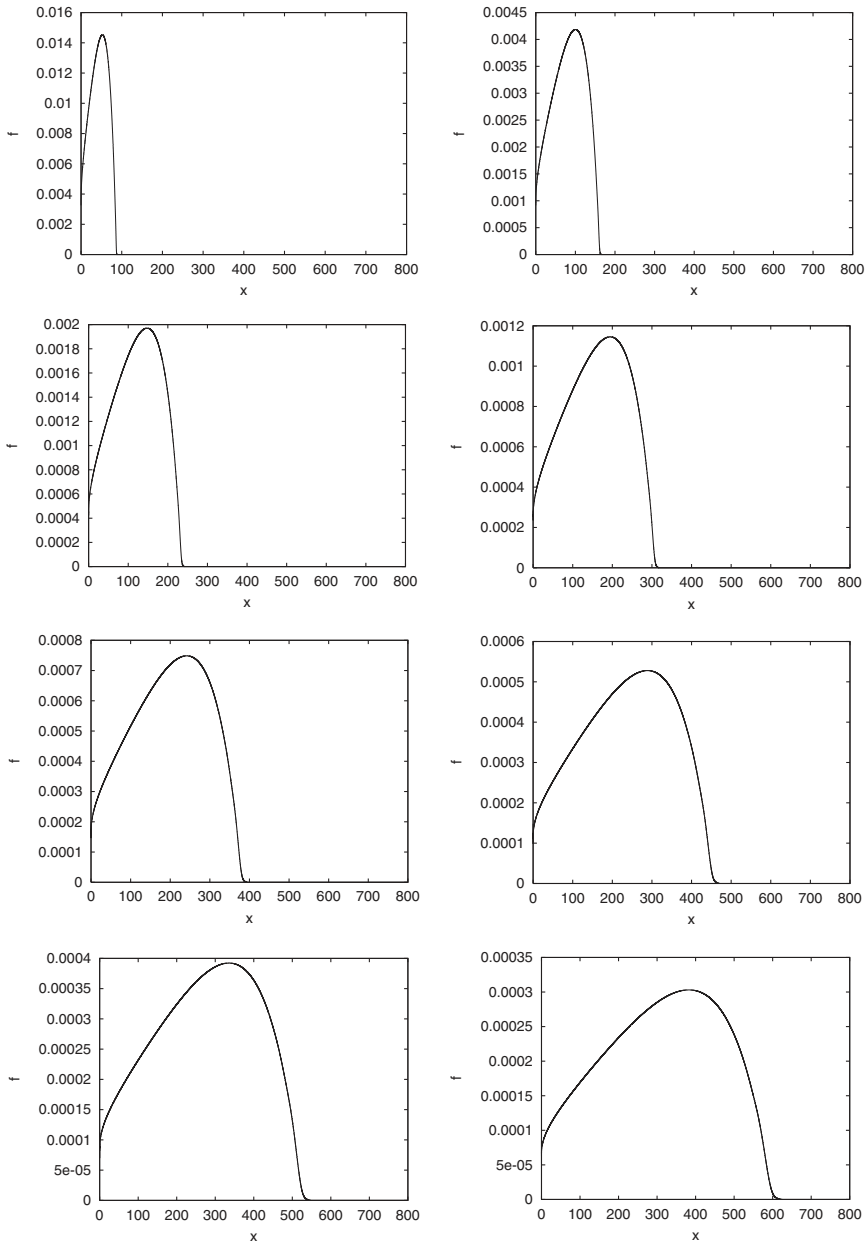

Fig. 15. Evolution of the triangle function initial data for the LS system every 250 time units.

function; a continuous non differentiable compactly supported initial data: a triangle function. For those initial data we have computed their evolution, the evolution of the concentration of monomers, the evolution of the total number of agglomerates and we have compared the final solution after 2000 units of time with stationary profiles. The results are given in Figs. 10 and 11 for the double Maxwellian, Figs. 12 and 13 for the step function and Figs. 14 and 15 for the triangle function.

We conclude from these figures the following observations:

1. A metastability region also appears for the concentration of monomers before $c(t)$ decreases. Note also that in the earlier stages of the evolution, the behavior of $c(t)$ is much more complicated for the double Maxwellian than for the single one.
2. A good agreement with the $t^{-1/3}$ law, as shown in the graph of $K(t) = t^{1/3}c(t)$. We can observe that the value to which $K(t)$ is converging depends on the initial data. In fact, for the double Maxwellian we observe values very close to $K_{\text{crit}} = 1.88988$, while

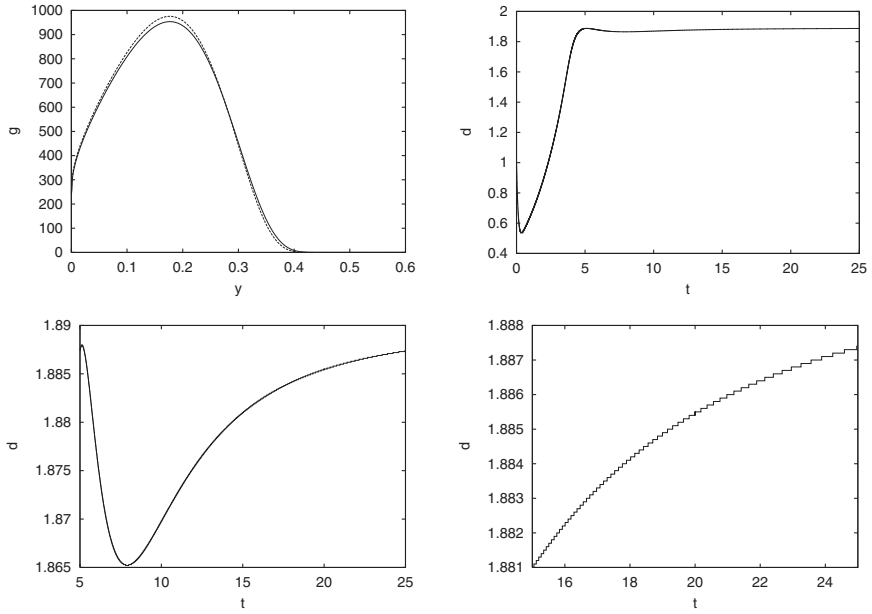

Fig. 16. Maxwellian initial data for the rescaled LS system: top left: Comparison between the computed solution after 25 time units (solid line) and the smooth LS profile M_{crit}; top right: $d(t)$ is converging towards $K_{\text{crit}} = 1.88988$; bottom left and bottom right: zooms of the graph of $d(t)$.

for the step function $K(t)$ is larger than this value, it continues to increase and is closer to the value $K = 2.05197$ for $p = 1$ given by (3.4). Also, for the triangle function $K(t)$ is larger than the critical value $K_{\text{crit}} = 1.88988$, continues to increase and is closer to the value $K = 1.95209$ for $p = 2$ given by (3.4).

3. m_0 decreases after the metastability region, in good agreement with the t^{-1} law.
4. The evolution of the solutions shows the solution $f(t, x)$ each 250 units of time. We can see clearly the stretching of the support and the convergence towards the shape of the corresponding stationary state given by formula (3.5).

Here, we have solved the LS system over the interval [0, 800] with 80 cells per unit length for the step and the triangle initial data and over the interval [0, 1000] with 40 cells per unit length for the double Maxwellian.

We have also made tests with functions having unbounded support and algebraic decay at infinity. The conclusions on the behavior of the

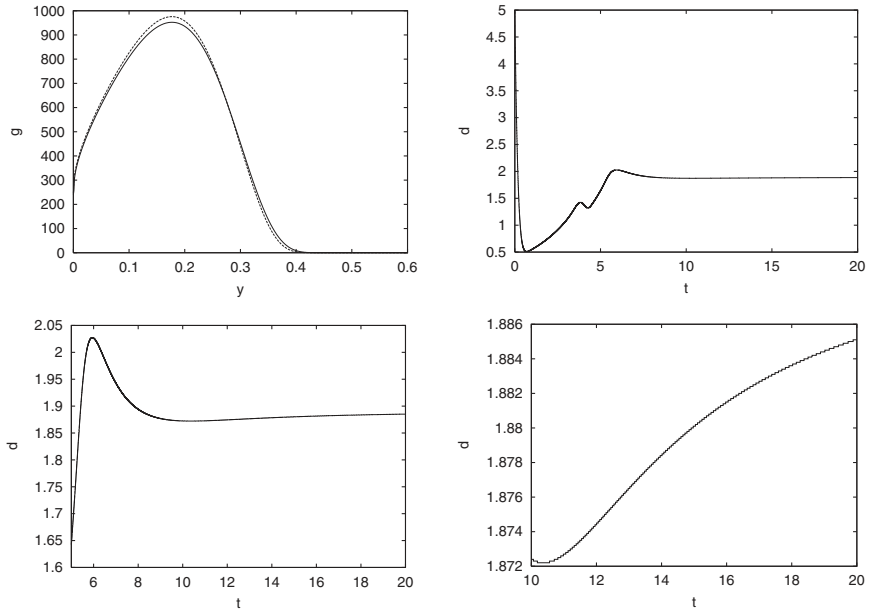

Fig. 17. Double Maxwellian initial data for the rescaled LS system: top left: Comparison between the computed solution after 20 time units (solid line) and the smooth LS profile M_{crit}; top right: $d(t)$ is converging towards $K_{\text{crit}} = 1.88988$; bottom left and bottom right: zooms of the graph of $d(t)$.

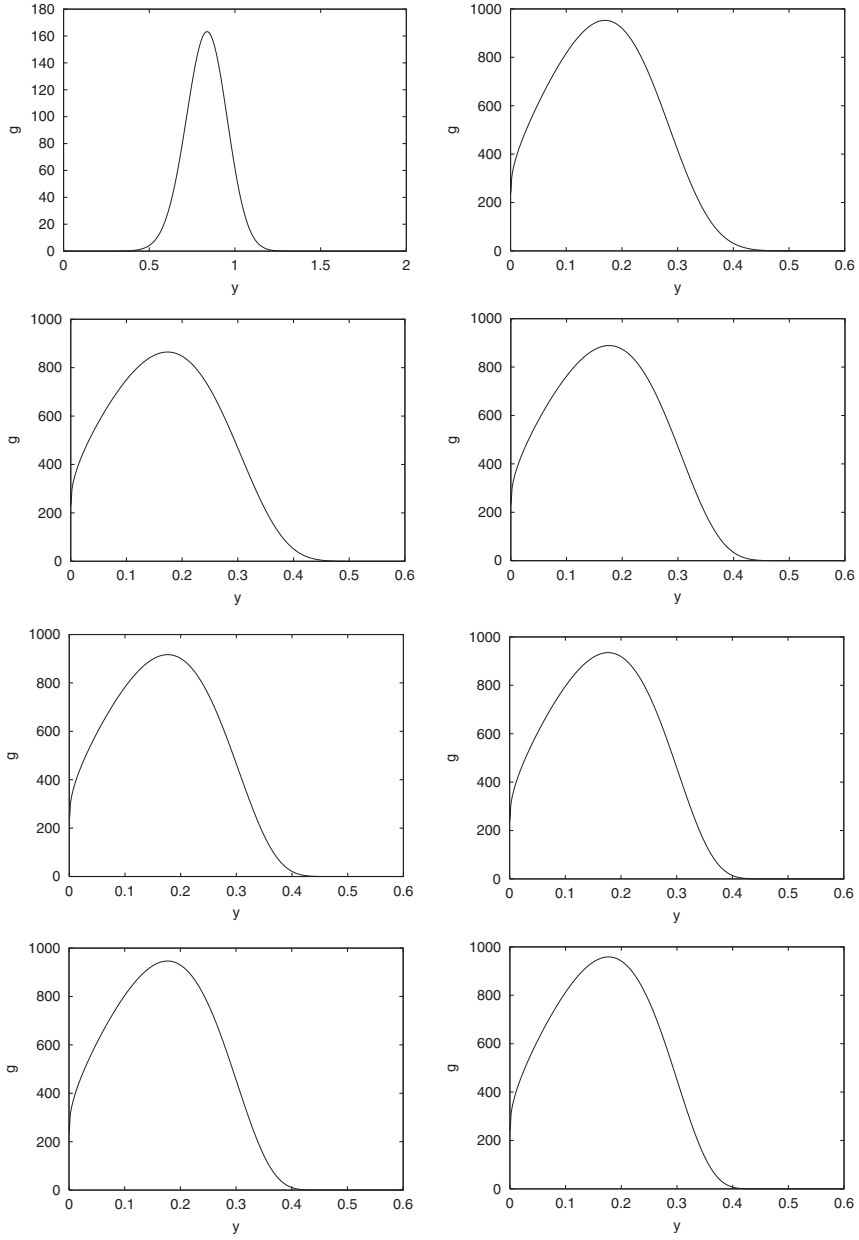

Fig. 18. Evolution of the Maxwellian initial data (see Fig. 3 bottom right) for the rescaled LS system every 2.5 time units.

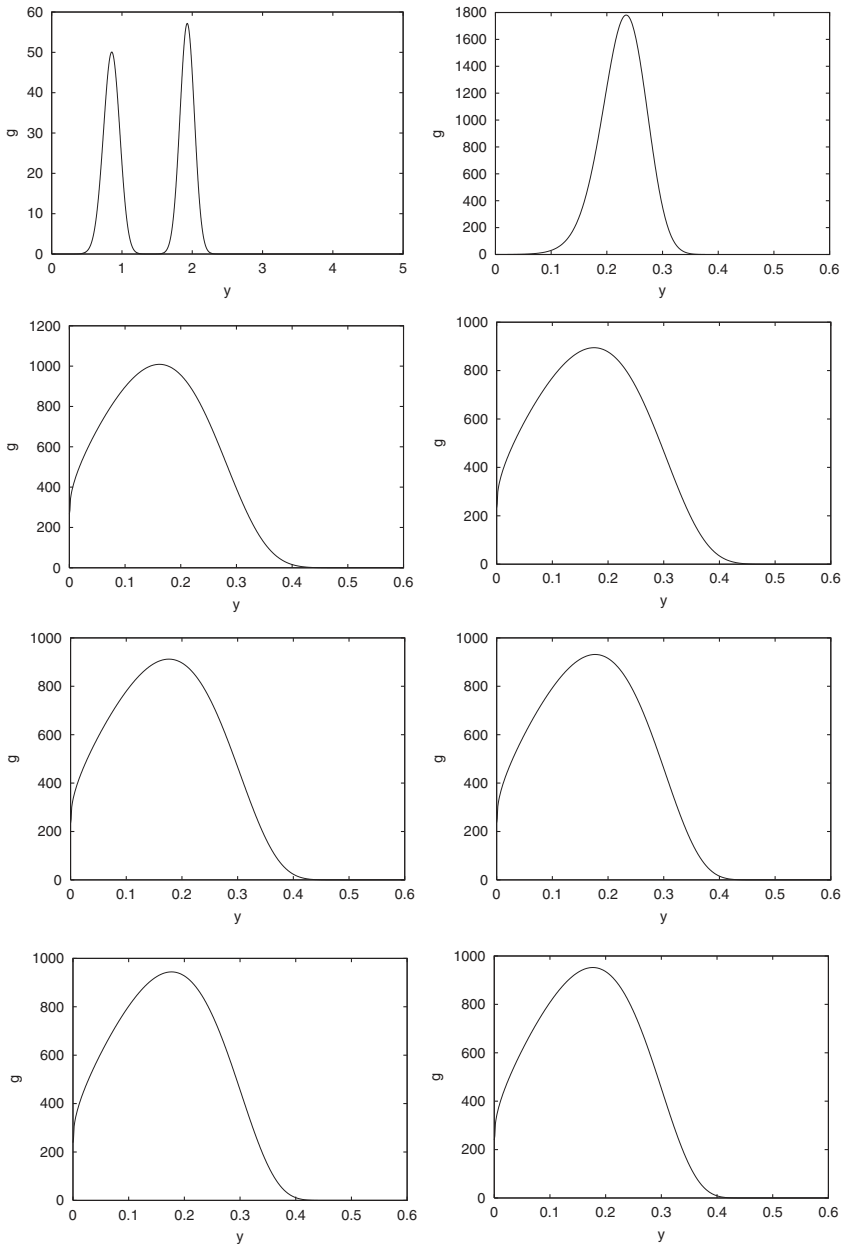

Fig. 19. Evolution of the double Maxwellian initial data for the rescaled LS system every 2.5 time units.

solution are the same as those for the Maxwellians and we do not deem necessary to include figures on that case. However, the remarkable point is the great sensitivity of the computation to the necessary truncation of the initial data. We should take under consideration a very large array of initial data, even with very small values in the last components, otherwise the solution could converge to the non smooth profile associated to the step function. This illustrates once again the high instability of the asymptotic profiles and the high influence of the tail of the initial data.

The crucial influence of the tail of the initial data is confirmed by the aggressive tests which consist of dealing with oscillating initial data. Figure 26 corresponds to the evolution, in rescaled variables, with the initial data

$$\frac{m}{\sqrt{2\pi\theta}} \exp(-(x-10)^2/(2\theta)) \times \sin^2(20x). \tag{4.2}$$

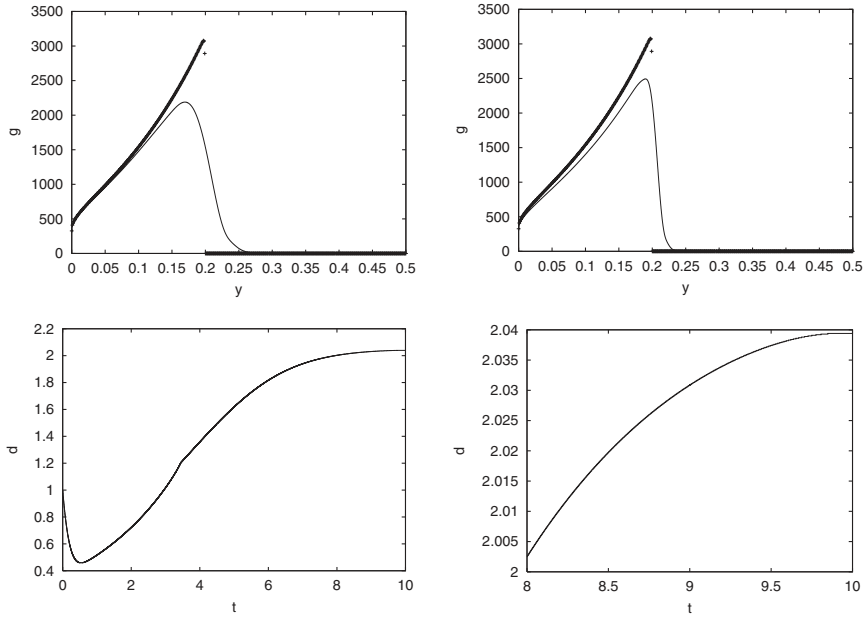

Fig. 20. Step function initial data for the rescaled LS system: top left: Comparison between the computed solution after 10 time units (solid line) and the asymptotic profile M_K with $K = 2.05197$; top right: Comparison between the computed solution after 9 time units (solid line) and the asymptotic profile M_K with $K = 2.05197$; bottom left and bottom right: $d(t)$ is converging towards $K = 2.05197$.

Figure 27 corresponds to the evolution with the initial data

$$\frac{m}{\sqrt{2\pi\theta}}\exp(-(x-10)^2/(2\theta))\times\frac{1}{1+0.1\sin(10x)}. \tag{4.3}$$

In both cases the solution does not converge to the smooth LS profile and instead is wandering around the smooth LS profile. Moreover, even the rescaled monomer concentration d is oscillating and does not stabilize. We point out that the CFL becomes prohibitive and does not allow to go further in time (but the final result presented here corresponds to e^{15} time units).

As a conclusion, we can assert that the conjectures CLS1–CLS4 are not verified in general: the large time behavior is highly dependent on the initial data. In particular, based on numerics, we find initial data for which conjectures CLS1–CLS3 are satisfied considering non universal constants. There are also initial data, with infinite support, for which we do not stabilize to the smooth profile.

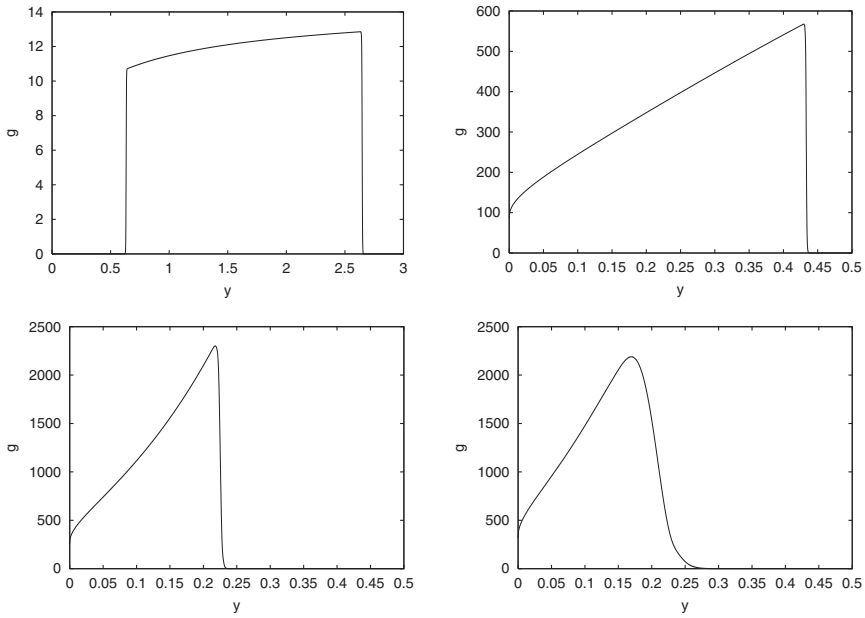

Fig. 21. Evolution of the step function initial data for the rescaled LS system every 2.5 time units.

4.2.3. Simulations on the Scaled Equation

Next, we consider the same set of initial data, but we perform the computations on the rescaled system. As mentioned before, the main advantage is to reduce the size of the domain of computation, since one avoids the stretching of the support of the solution in the new variables.

The price to be paid comes from a considerable increase of the stiffness of the problem, in particular when dealing with the non regular data. This requires one to observe carefully the CFL condition; otherwise undesirable oscillations can be observed on the computed solutions. These oscillations arise mainly from the end of the support, while d is also oscillating, illustrating again the crucial role played by the largest aggregates. Note that the computational time are comparable to those for the original system, but the rescaled variables are well adapted to go further in time. Let us recall that the variable τ is a logarithmic scale of the variable t.

Results for the Maxwellian and the double Maxwellian can be found in Figs. 16–18 and Figs. 17–19, respectively. We recover the same conclusions as with the original variables, and the convergence to the expected

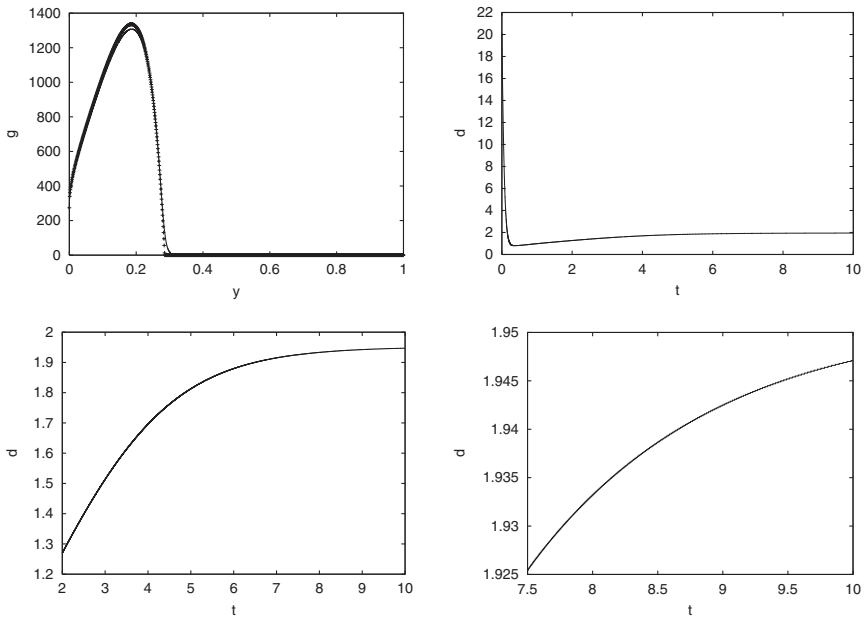

Fig. 22. Triangle function initial data for the rescaled LS system: top left: Comparison between the computed solution after 10 time units (solid line) and the asymptotic profile M_K with $K = 1.95209$; top right: $d(t)$ is converging towards $K = 1.95209$; bottom left and bottom right: zooms of the graph of $d(t)$.

smooth profile. Let us remark that in this computation we have arrived at $\tau = 25$ and $\tau = 20$, respectively, rescaled time units which correspond to the order of 10^{11} and 10^9 original time units. Therefore, we have gone much further with respect to the simulations in the original system.

Then, Figs. 20–23 show the results of the computations for the step function and the triangle as initial data, respectively. Here, we have arrived at $\tau = 10$ rescaled time units which correspond to the order of 10^5 original time units.

Again, one verifies the convergence to the asymptotic profile M_K with the value of K corresponding to the behavior of the data at the end of its support. However, the problem becomes very stiff as the regularity at the end of the support gets smeared. It should be noted that smearing effects induced by the numerical approximation become noticeable at these very large time for the largest aggregates.

Consequently, while the solution is very close to the profile M_K, it finally deteriorates and converges to the smooth profile, as observed by Fig. 20 top, and Fig. 23 bottom right. This fact illustrates the enormous numerical difficulty in preserving the precise behavior of the solution at the

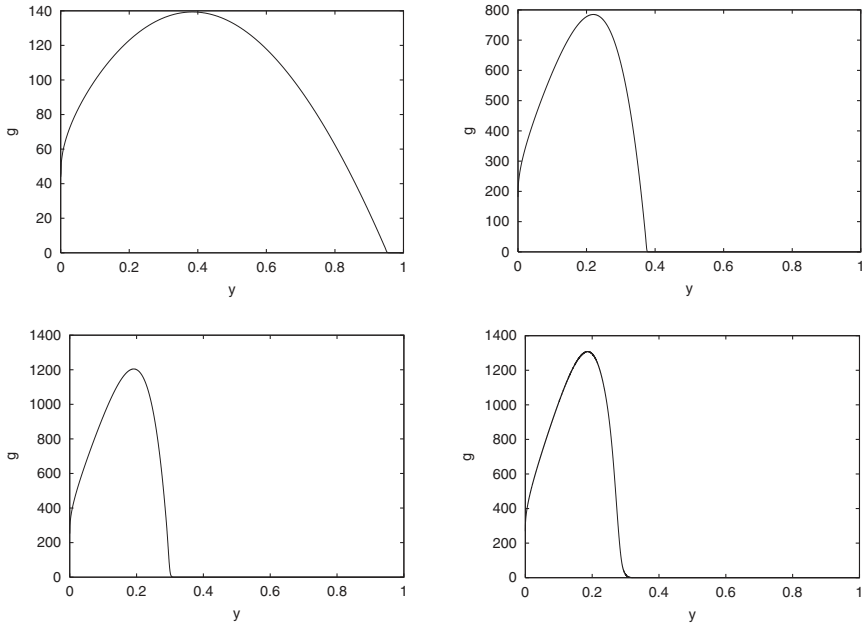

Fig. 23. Evolution of the triangle function initial data for the rescaled LS system every 2.5 time units.

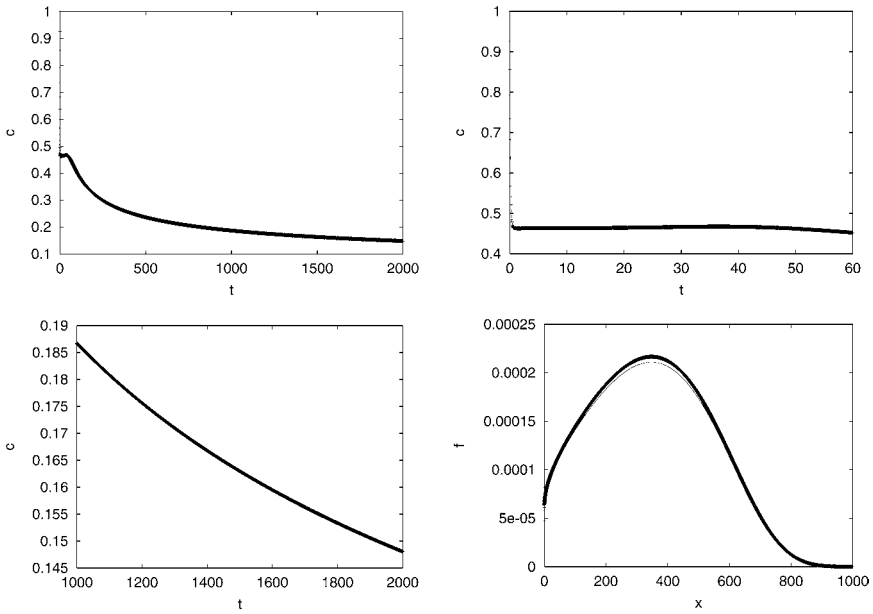

Fig. 24. Maxwellian initial data for the LSW system: top right, left and bottom left: Comparison between monomer concentration $c(t)$ for the LS and the LSW; bottom right: Comparison between the computed solutions for the LS and LSW after 2000 time units.

tip of the support as time becomes very large, and thus, capturing the right asymptotic profile. We have solved the rescaled LS system over the interval [0, 30] with 1000 cells per unit length.

4.2.4. Simulations on the LSW Equation

Our final tests are devoted to the LSW system, the number of cells and numerical issues are chosen in the same way as for the corresponding cases of the LS system. The results showed in Fig. 24 and 25 confirm that this system can be seen as a good approximation of the original one for large time, as $c(t)$ has become small, in agreement with the theoretical results in [15]; it also agrees with the prediction proposed in [22] since we recover again the asymptotic profile which corresponds to the behavior of the initial data at the end of its support.

5. CONCLUSION

The main conclusion of our numerical study is that the asymptotic behavior of the solutions of the Lifshitz–Slyozov system depends on the

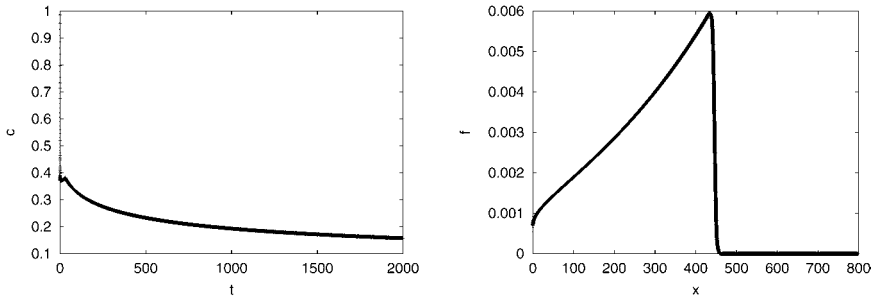

Fig. 25. Step initial data for the LSW system: left: Comparison between monomer concentration $c(t)$ for the LS and the LSW; right: Comparison between the computed solutions for the LS and LSW after 2000 time units.

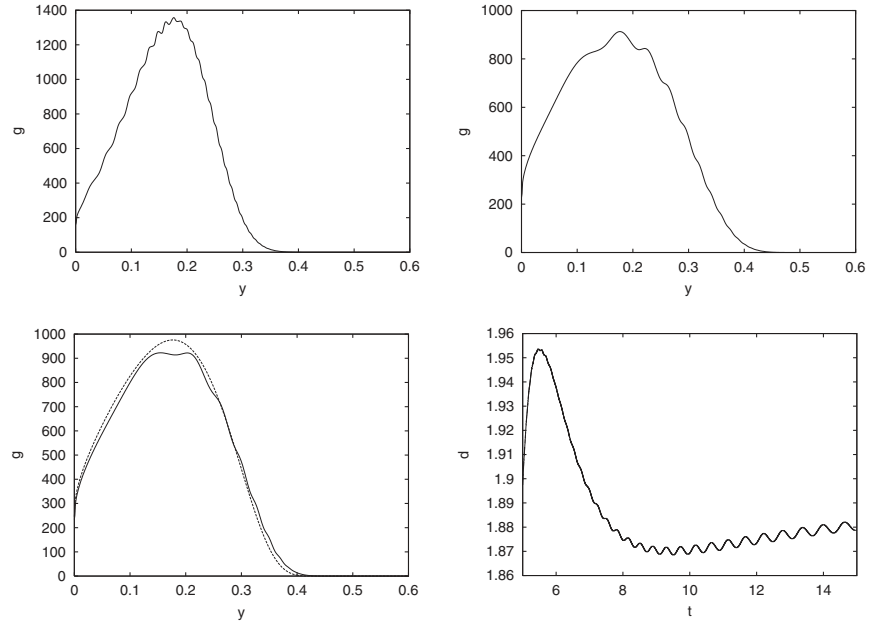

Fig. 26. Perturbation of the Maxwellian initial data for the LS system in (4.2): top left: after 5 time units, top right: after 15 time units, bottom left: comparison after 15 time units with the LS smooth profile, bottom right: monomer concentration.

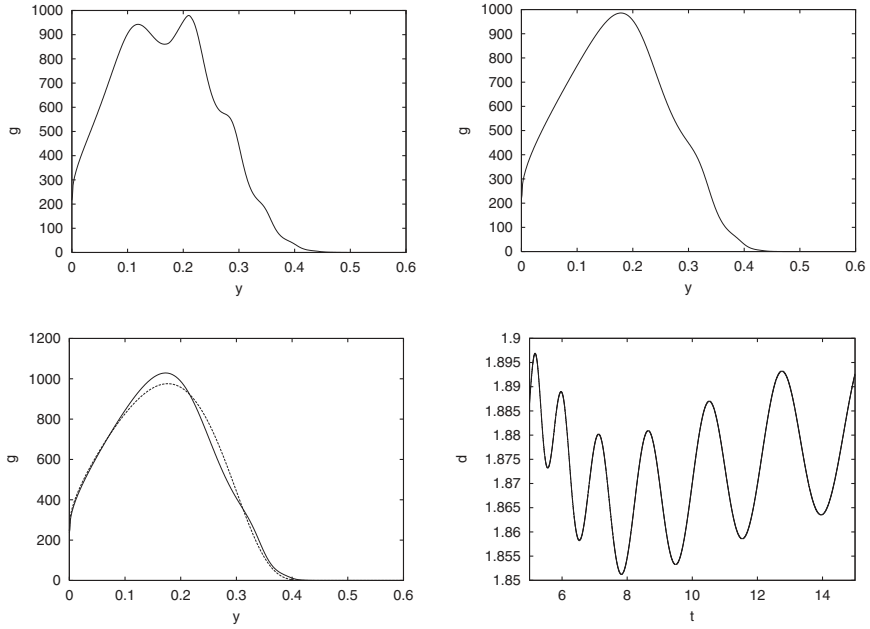

Fig. 27. Perturbation of the Maxwellian initial data for the LS system in (4.3): top left: after 5 time units, top right: after 15 time units, bottom left: comparison after 15 time units with the LS smooth profile, bottom right: monomer concentration.

initial data. Of course, the challenging question remains to exhibit some condition that guarantee the convergence towards the smooth profile as conjectured in [18]. We expect that our investigation will highlight some elements for finding a solution. First, the convergence to 0 of the monomer concentration certainly does not hold for any initial repartition of mass. Roughly speaking, a certain amount of mass should be given by aggregates larger than the initial critical size. Next, even in situations where $c(t)$ goes to 0, monotonicity is far from clear; in any case it does not concern the earlier stages of evolution where c can have a complicated behavior.

In our tests, when $c(t) \to 0$, we also verify that $c(t)\, t^{1/3}$ goes to a constant K. However, the constant depends on the distribution of the largest aggregates present initially in the solution. Accordingly, conjectures CLS1–CLS3 may hold under additional assumptions on the initial data, but with a constant K which depends on the shape of the initial data f_0 and the final profile preserves some memory of the initial shape of the density. Convergence towards the smooth LS profile for several non compactly supported initial data is numerically observed. These results bring up the question referred above of finding sufficient conditions on positive fast

decaying at infinity initial data such that their evolution leads towards the smooth LS profile.

Let us finally mention that some questions raised in this study have rigorously been answered in a very recent work [23]. Despite this fact, our numerical scheme is shown to be a suitable numerical method to solve the LS system and sheds some light on several facts not included in [23].

ACKNOWLEDGMENTS

Partial support from the Spanish DGI-MCYT project BFM2002-01710 and the TMR Project "Asymptotic Methods in Kinetic Theory," grant number ERB-FRMXCT-970157 are gratefully acknowledged. Part of this work was done while J. A. Carrillo was visiting Laboratoire J. A. Dieudonné, UMR 6621, University Nice Sophia Antipolis and T. Goudon was visiting the Department of Applied Math., University of Granada. We thank both for their hospitality.

REFERENCES

1. Ball, J., Carr, J., and Penrose, O. (1986). The Becker–Döring cluster equations: Basic properties and asymptotic behavior of solutions. *Comm. Math. Phys.* **104**, 657–692.
2. Becker, R., and Döring, W. (1935). Kinetische behandlung der keimbildung in ubersattigten damfern. *Ann. Phys. (Leipzig)* **24**, 719–752.
3. Brown, L. (1989). A new examination of classical coarsening theory. *Acta Metall.* **37**, 71–77.
4. Carr, J., and Penrose, O. (1998). Asymptotic behavior of solutions to a simplified Lifshitz–Slyozov equation. *Phys. D* **124**, 166–176.
5. Carrillo, J. A., Gamba, I. M., and Shu, C. W. (2000). Computational macroscopic approximations to the 1-D relaxation-time kinetic system for semiconductors. *Physica D* **146**, 289–306.
6. Chen, M., and Voorhees, P. (1993). The dynamics of transient Ostwald ripening. *Modelling Simul. Mater. Sci. Eng.* **1**, 591–612.
7. Collet J. F., Goudon T. (2000). On solutions of the Lifshitz–Slyozov model. *Nonlinearity* **13**, 1239–1262.
8. Collet, J. F., and Goudon, T. (1999). Lifshitz–Slyozov equations: The model with encounters. *Transp. Theory Stat. Phys.* **28**, 545–573.
9. Collet, J. F., Goudon, T., Poupaud, F., and Vasseur, A. (2002). The Becker–Döring system and its Lifshitz–Slyozov limit. *SIAM J. Appl. Math.* **62**, 1488–1500.
10. Collet, J. F., Goudon, T., and Vasseur, A. (2002). Some remarks on the large-time asymptotic of the Lifshitz–Slyozov equations. *J. Stat. Phys.* **108**, 341–359.
11. Dadyburjor, D. B., and Ruckenstein, E. (1977). Kinetics of Ostwald ripening. *J. Crystal Growth* **40**, 279–290.
12. Filbet, F., and Laurençot, P. (2002). Numerical approximation of the LSW equations, Preprint.
13. Jiang, G., and Shu, C.W. (1996). Efficient implementation of weighted ENO schemes. *J. Comp. Physics* **126**, 202–228.

14. Laurençot, P. (2001). Weak solutions to the Lifshitz–Slyozov–Wagner equation. *Indiana Univ. Math. J.* **50**, 1319–1346.
15. Laurençot, P. (2001). The Lifshitz–Slyozov–Wagner equation with conserved total volume, Preprint.
16. Leveque, R.J. (1992). *Numerical Methods for Conservation Laws*, Birkhäuser.
17. Lifshitz, I. M., and Pitaevski, L. (1990). *Cinétique Physique*, Coll. Physique Théorique, Landau–Lifshitz, Mir.
18. Lifshitz, I. M., and Slyozov, V. V. (1961). The kinetics of precipitation from supersaturated solid solutions. *J. Phys. Chem. Solids* **19**, 35–50.
19. Meerson, B., and Sasorov, P. (1996). Domain stability, competition, growth, and selection in globally constrained bistable systems. *Phys. Rev. E* **53**, 3491–3494.
20. Ostwald, W. (1900). *Z. Phys. Chem.* **34**, 495.
21. Niethammer, B., and Pego, R. (2000). On the initial-value problem in the Lifshitz–Slyozov–Wagner theory of Ostwald ripening. *SIAM J. Math. Anal.* **31**, 467–485.
22. Niethammer, B., and Pego, R. (1999). Non-self-similar behavior in the LSW theory of Ostwald ripening. *J. Stat. Phys.* **95**, 867–902.
23. Niethammer, B., and Pego, R. (2001). The LSW model for domain coarsening: Asymptotic behavior for conserved total mass. *J. Stat. Phys.* **104**, 1113–1144.
24. Penrose, O. (1997). The Becker–Döring equations at large times and their connection with the LSW theory of coarsening. *J. Stat. Phys.* **89**, 305–320.
25. Sagalovich, V. V., and Slyozov, V. V. (1987). Diffusive decomposition of solid solutions. *Sov. Phys. Usp.* **30**, 23–44.
26. Shu, C. W., and Osher, S. (1988). Efficient implementation of essentially non-oscillatory shock-capturing schemes. *J. Comput. Phys.* **77**, 439–471.
27. Shu, C. W. (1998). Essentially non-oscillatory and weighted essentially non-oscillatory schemes for hyperbolic conservation laws, *Advanced Numerical Approximation of Nonlinear Hyperbolic Equations*, B. Cockburn, C. Johnson, C.-W. Shu, and E. Tadmor (A. Quarteroni, ed.), Lecture Notes in Mathematics, Vol. 1697, Springer, pp. 325–432.
28. Sonnendrucker, E., Roche, J., Bertrand, P., and Ghizzo, A. (1999). The semi-Lagrangian method for the numerical resolution of the Vlasov equation. *J. Comput. Phys.* **149**, 201–220.
29. Wagner, C. (1961). Theorie der Alterung von Niederschlägen durch Umlösen (Ostwald-Reifung). *Z. Elektrochem.* **65**, 581–594.